CHARACTERIZATION OF ALGINATE SCAFFOLDS USING X-RAY IMAGING TECHNIQUES

A Thesis Submitted to the College of

Graduate Studies and Research

in Partial Fulfillment of the Requirements

for the Degree of Master of Science

in the Division of Biomedical Engineering

University of Saskatchewan

Saskatoon

By

Yijing Guan

PERMISSION TO USE

In presenting this thesis in partial fulfillment of the requirements for a Postgraduate degree from the University of Saskatchewan, I agree that the Libraries of this University may make it freely available for inspection. I further agree that permission for copying of this thesis in any manner, in whole or in part, for scholarly purposes may be granted by the professor or professors who supervised my thesis work or, in their absence, by the Head of the Department or the Dean of the College in which my thesis work was done. It is understood that any copying or publication or use of this thesis or parts thereof for financial gain shall not be allowed without my written permission. It is also understood that due recognition shall be given to me and to the University of Saskatchewan in any scholarly use which may be made of any material in my thesis.

Requests for permission to copy or to make other uses of materials in this thesis in whole or part should be addressed to:

Head of the Division of Biomedical Engineering
University of Saskatchewan
Saskatoon, Saskatchewan
S7N 5A9
Canada

ABSTRACT

Alginate is a popular biomaterial in tissue engineering. When crosslinked with calcium ions (Ca^{2+}), alginate forms a hydrogel which provides necessary mechanical support as a scaffold. The material properties as well as the biological properties of alginate scaffold are of great importance. In this thesis, the aim is to use traditional methods, such as scanning electron microscopy (SEM) and light microscopy, and emerging X-ray imaging techniques, such as micro-computed tomography (micro-CT) and synchrotron radiation (SR) X-ray imaging, to characterize the alginate scaffolds. Firstly, the material properties of freeze-dried alginate scaffolds were evaluated using micro-CT, as it is a non-destructive and non-invasive imaging method, and can provide three-dimensional information. Alginate scaffolds made with different sodium alginate concentrations and frozen to different temperatures were scanned and analyzed in micro-CT. Results indicated that lower freezing temperature and higher sodium alginate concentration lead to smaller pore size and porosity. Secondly, cell culture experiments were carried out to study the biological properties and the interactions of alginate hydrogel with cells. A Schwann cell line was either blended with alginate solution before crosslinking with calcium chloride ($CaCl_2$) or put around alginate gel in the culture dish. Light microscopy of sectioned slices showed that cells surrounding the alginate gel could not grow into the gel, while cells blended with alginate solution before crosslinking could proliferate inside the hydrogel. Cells grown inside a thin slice of alginate gels appeared to be in better condition and were larger in size and also grew in clusters. Thirdly, in order to image soft tissue buried inside alginate gels, such as brain slices, novel imaging methods based on synchrotron radiation (SR) were applied, such as absorption and phase contrast imaging, diffraction-enhanced imaging (DEI) and also combined with computed tomography (CT). Synchrotron-based monochromatic X-ray imaging proved to be good at distinguish objects of similar density, especially biological soft tissue samples, even without any staining material, such as osmium tetroxide (OsO_4). These three pieces of research work show the potential in applying the emerging X-ray imaging in soft tissue engineering.

ACKNOWLEDGMENTS

I would like to extend sincere thanks to my supervisors, Dr. Daniel Chen and Dr. Dean Chapman, for their guidance and support during this research work. Without their great efforts, this work would be impossible. I am grateful to my committee members, Dr. David Schreyer and Dr. David Cooper, for their unending patience in instructing me in micro-CT operations, software analysis, biological experiments and cell culture, and for their inspiring ideas. My thanks are also extended to BMIT scientists, Dr. Tomasz Wysokinski and Dr. George Belev, for their assistance in setting up and configuring beamline for imaging. I would like to express my gratitude to technicians, Dr. Guosheng Liu for his instruction in SEM, and Ms. Tangyne Berry for preparing Schwann cell line cultures. A special thank-you is extended to all the colleagues in the Tissue Engineering Research Group. The warm atmosphere and team work spirit inspired my work.

The present work was financially supported by the Saskatchewan Health Research Foundation (SHRF) and the Natural Science and Engineering Research Council (NSERC) of Canada.

TABLE OF CONTENTS

LIST OF TABLES

LIST OF FIGURES

LIST OF ABBREVIATIONS

BM:	bending magnet
BMIT:	Biomedical Imaging and Therapy
CLS:	Canadian Light Source
DEI:	diffraction-enhanced imaging
DMEM:	Dulbecco's Modified Eagle Medium
FBP:	filtered-back projection
FBS:	fetal bovine serum
FOV:	field of view
micro-CT:	micro-computed tomography
PBS:	Phosphate buffer solution
PF:	Para-formaldehyde
PNS:	peripheral nervous system
PNI:	peripheral nerve injury
ROI:	Region of Interest
SD:	sample-to-detector distance
SEM:	scanning electron microscope
SR:	synchrotron radiation
SR μCT:	synchrotron radiation micro-computed tomography

1 INTRODUCTION

1.1 Background

1.1.1 Tissue Engineering

Tissue engineering is the application of cells, engineering and materials methods, and suitable biochemical growth factors to improve the fundamental understanding of structure-function relationships in a biological environment, and to develop biological substitutes that restore, maintain or improve tissue function. In effect, cells could be isolated from a healthy site of the patient, expanded in vitro and/or modified by gene therapy to replace a defective gene, and then re-implanted back into the patient under conditions to correct the functional defect (Figure 1). Therefore, the surgeon can potentially adapt these fundamental techniques of tissue engineering with the tools of minimally invasive surgery to bring a new concept of disease treatment [1-3]. Tissue engineering can surpass the limitation of donation shortage, and also eliminate immunological reactions.

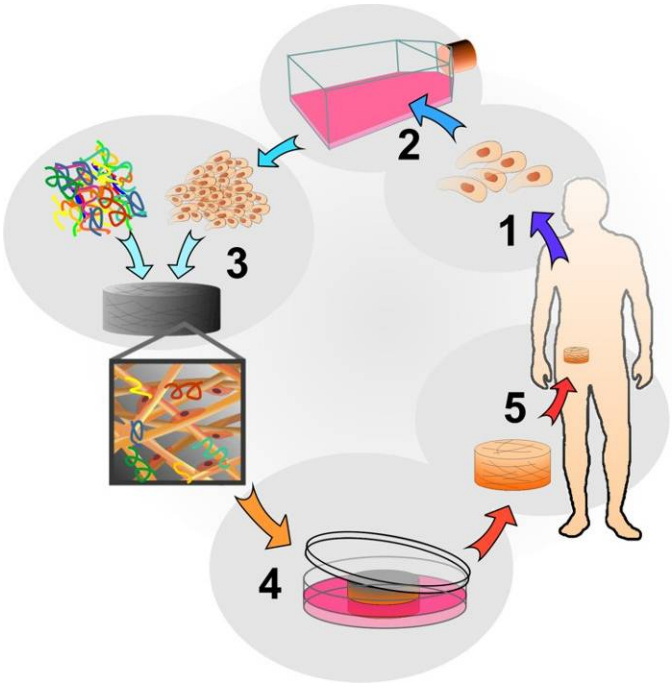

Figure 1: The central tissue engineering paradigm [4]

1.1.2 Scaffolds

Tissue engineered scaffolds are designed and fabricated for supporting cell migration, cell growth and differentiation, and guiding tissue development and organization into a mature and healthy state. Scaffolds in tissue-engineered constructs will have certain minimum requirements for biochemical, chemical and physical properties. Firstly, any scaffold must provide sufficient initial mechanical strength and stiffness to substitute for the mechanical function of the diseased or damaged tissue that it aims at repairing or regenerating. Secondly, scaffolds must be made with materials of good biocompatibility and biodegradability so that they do not negatively interact with tissue nearby and stay structurally stable until new tissue is formed.

A biomaterial is a material intended to interface with biological systems to evaluate, treat, and augment, or replace any tissue, organ or function of the body. There are different kinds of biodegradable and biocompatible biomaterials used for tissue engineered scaffolds. Natural biopolymers, including collagen, chitosan, alginate and silk, are widely used as they are derived naturally from a biological environment and have excellent biocompatibility. Synthetic polymers are made to substitute for natural biopolymer but can have lower biocompatability. Synthetic polymers include polylactides, polycaprolactone, polyurethanes and others. In this thesis, a natural polymer of alginate is used. Alginate is a gel that has several potential medical applications but with a variability in biocompatibility characteristics and biological performances[5, 6]. It is a biological material derived from sea algae, composed of linear block copolymers of 1-4 linked b-D-mannuronic acid (M) and a-L- guluronic acid (G) (Figure 2). Alginate can be ionically cross-linked by the addition of divalent cations (like Ca^{2+}) in aqueous solution. The gelation and cross-linking of the polymers are mainly achieved by the exchange of sodium ions from the guluronic acids with the divalent cations, and the stacking of these guluronic groups to form the characteristic egg-box

structures[7, 8]. Scaffolds made of alginate crosslinked with calcium chloride ($CaCl_2$) can support cells and provide pores for them to penetrate through [9].

Figure 2: Structural of alginate acid

A number of fabrication technologies have been applied to process biocompatible and biodegradable scaffolds. Conventional techniques include porogen leaching, gas foaming, phase separation, melt moulding and freeze drying [10]. In this thesis, the freeze drying technique is applied to characterize the micro-structure of alginate scaffolds. Freeze drying is also known as lyophilization or cryodesiccation. It is a dehydration process by freezing the material and then reducing the surrounding pressure and adding enough heat to allow the frozen water in the material to sublime directly from the solid phase to the gas phase [11].

Several requirements have been identified as crucial for the production of tissue scaffolds. These include that the scaffold: 1) be highly porous to allow cell growth and movement as well as the transport of nutrients and metabolic waste; 2) be biocompatible and biodegradable to match cell/tissue growth in vitro and/or in vivo; 3) have suitable surface chemistry for cell attachment, proliferation, and differentiation; and 4) have mechanical properties matching those of tissues at the site of implantation [12]. Thus morphology and micro-structure of scaffolds, such as pore size, porosity, interconnectivity and wall thickness, are of crucial importance. A pore can be defined as a void space within a scaffold, whereas porosity can be considered as the percentage of a collection of pores (pore volume fraction). Macro-pores (i.e. above 50 microns) are of a scale to influence tissue function. Micro-pores (i.e. below 50 microns)

are of a scale to influence cell function (e.g. cell attachment) given that mammalian cells typically are 10-20 microns in size. Nano-porosity refers to pore architectures or surface textures on a nano-scale (i.e. 1-1000 nm). Interconnectivity of pores is the state of open pores. As interconnected pores enable cell migration and proliferation freely inside scaffold, this property is a critical factor in scaffold design and characterization. It is preferable that scaffolds for tissue engineering have 100% interconnecting pore volume, thereby also maximizing the diffusion and exchange of nutrients throughout the entire scaffold volume [4].

Cells in culture lack the ability to assemble into three-dimensional (3D) structures and thus recreate the anatomical shape of the tissue. Instead, they randomly migrate to form a two dimensional (2D) layer of cells. However, as 3D tissues are required, cells are seeded onto porous matrices or encapsulated inside scaffolds where they attach and colonize to form new tissue.

1.1.3 Schwann Cells

Schwann cells are glia of the peripheral nervous system (PNS) that wrap around the axon to form the myelin sheath. Schwann cells are the principle neuroglial cells in the PNS. They produce myelin, which has important effects on the speed of transmission of electrical signals. They also enhance the regeneration of axons in both the central nervous system (CNS) [13] and the peripheral nervous system [14]. In spinal cord injury, they can reduce the size of spinal cysts, remyelinate axons and enhance functional recovery. Schwann cells produce a number of growth factors that support the growth of axons, including nerve growth factor (NGF), brain-derived neurotrophic factor (BDNF), ciliary neurotrophic factor (CNTF), neurotrophin-3 (NT-3), conserved dopamine neurotrophic factor (CDNF) and fibroblast growth factor (FGF). They also express axon guidance cell adhesion molecules on their surfaces. In peripheral nerve injury, Schwann cells in the distal stump undergo proliferation

and phenotypical changes to prepare the local environment for axonal regeneration. By elaborating basement membrane that contains many extracellular matrix proteins, Schwann cells can improve nerve regeneration.

1.1.4 Scanning Electron Microscope

The Scanning Electron Microscope (SEM) is a type of electron microscope that images the sample surface by scanning it with a high-energy beam of electrons in a raster scan pattern. The electrons interact with the atoms that make up the sample producing signals that contain information about the sample's surface topography, morphology, composition and crystallographic information. SEM can produce very high-resolution images of a sample surface, revealing details about 1 to 5 nm in size and has a very large depth of field yielding a characteristic three-dimensional appearance useful for understanding the surface structure of a sample.

In a typical SEM, an electron beam is thermionically emitted from an electron gun fitted with a tungsten filament cathode. Tungsten is normally used in thermionic electron guns because it has the highest melting point and lowest vapor pressure of all metals, thereby allowing it to be heated for electron emission, and because of its low work function and low cost. Other types of electron emitters include lanthanum hexaboride (LaB_6) cathodes, which can be used in a standard tungsten filament SEM if the vacuum system is upgraded and field emission guns (FEG), which may be of the cold-cathode type using tungsten single crystal emitters or the thermally-assisted Schottky type, using emitters of zirconium oxide. The electron beam, which typically has an energy ranging from a few hundred eV to 40 keV, is focused by one or two condenser lenses to a spot about 0.4 nm to 5 nm in diameter. The beam passes through pairs of scanning coils or pairs of deflector plates in the electron column, typically in the final lens, which deflect the beam in the x and y axes so that it scans in a raster fashion over a rectangular area of the sample surface.

Nearly all samples require some type of preparation before examination in the SEM. Samples must be: (1) devoid of water, solvents, or other materials that could vaporize in the vacuum and either contaminate the column or cause vacuum problems. Biological samples, such as living cells and tissues, are usually dehydrated by critical point drying, which involves replacement of water in the cells with organic solvents such as ethanol or acetone, and replacement of these solvents in turn with a transitional fluid such as liquid carbon dioxide at high pressure. The carbon dioxide is finally removed while in a supercritical state, so that no gas-liquid interface is present within the sample during drying; (2) firmly mounted on metal holders called stubs. Stubs are usually made of aluminum. Samples are usually fastened to the stub by glues and tapes; and (3) electrically conductive. Samples must be coated for conductivity to prevent the accumulation of electrostatic charge at the surface. The most common coating material is gold, deposited on the sample either by low vacuum sputter coating or by high vacuum evaporation [15].

1.1.5 Micro-computed Tomography

Micro-computed tomography (micro-CT) is a medical imaging method employing tomography created by computer processing and can reach a spatial resolution up to micro-meter level. In conventional radiography, when X-ray penetrates through a human body, it gets attenuated and provides a two-dimensional image according to different absorption. The drawback is that the three-dimensional volume of a human body is compressed into a 2D image. All underlying bone structures and tissues are superimposed, which results in significant reduction of visibility of the object of interest. However, with computed tomography (CT), a single plane can be photographed, with the outline of structures in other planes eliminated. More details can be revealed in this way [16]. Micro-CT has been wildly applied in the biomedical field due to its merits of 3D visualization, high resolution imaging and non-destructive

sample preparation. In tissue engineering, micro-CT is commonly used in bone tissue engineering to study neovascularization. As bone has good X-ray absorption, micro-CT can reveal details inside bone structures and provide 3D information [17].

1.1.6 SR X-ray Imaging Methods

Although SR X-ray imaging does not have spatial resolution as high as SEM (up to nano scale), it can penetrate through thick samples and even the human body. Also, it can deliver fully quantitative, isotropic 3D data, due to its high brilliance and monochromatic radiation. There are several major techniques in SR X-ray imaging, including SR absorption contrast imaging, in-line phase contrast imaging, and diffraction-enhanced imaging (DEI). SR X-ray imaging can also be combined with micro-computed tomography and result in synchrotron radiation micro-computed tomography (SR μCT).

SR absorption contrast imaging has a similar setup (Figure 3) as the traditional clinical radiology using X-ray coming from the X-ray tube. An incoming white synchrotron beam incidents on double crystal monochromators in order to select the desired wavelength. Then the beam goes through the object and hits on the planar detector. SR absorption contrast imaging utilizes the differences in linear absorption coefficient within the object being imaged and obtains the attenuation contrast on the detector.

In-line phase contrast imaging (Figure 4) has a similar setup as SR absorption contrast imaging, except that the distance between the sample and the detector is much larger, usually in a range from tens of centimeters to several meters. In SR absorption contrast imaging, due to the fact that the detector is usually placed close to the object, the bending of beam is not so obvious and the attenuation of beam absorbed by the object is the major contrast. However,

when the detector is placed to a larger distance from the object, the bending of beam (refraction) is prominent and thus results in sharper contrast near the edges. The contrast resulting from refraction is much more notable than attenuation contrast [18]. Figure 5 [19] shows the difference between absorption and phase contrast imaging. Phase contrast imaging greatly enhances the differences among soft tissues, such as normal tissue and a cancer lesion, which have quite similar absorption coefficients and cannot be distinguished by absorption imaging. Also, phase contrast imaging can be used to reveal the tissue structures without using contrast agents [20, 21].

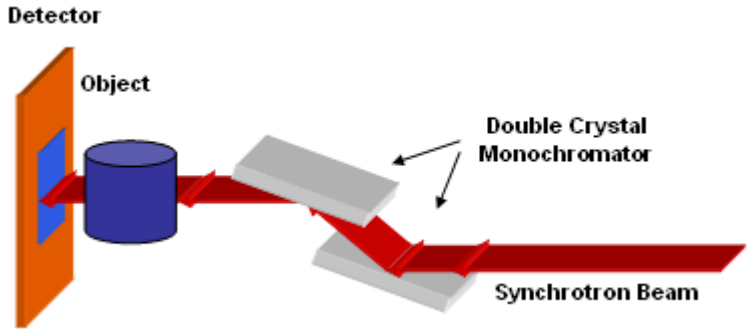

Figure 3: Schematic of SR absorption contrast imaging setup

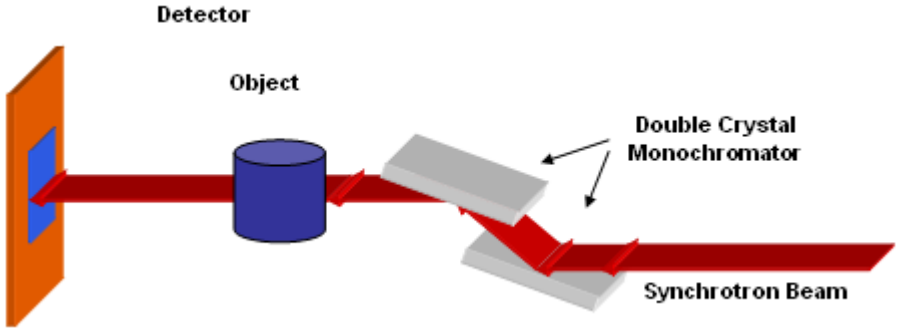

Figure 4: Schematic of in-line phase contrast imaging setup

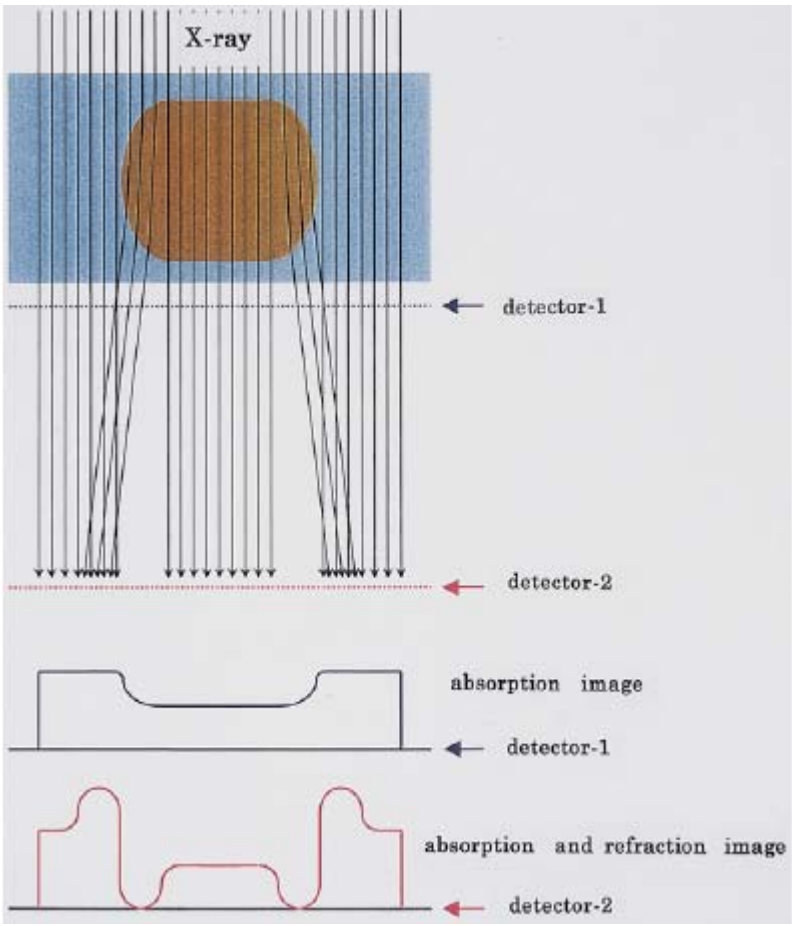

Figure 5: Diagram illustrates the principle of refraction and absorption images [19]

Diffraction Enhanced Imaging (DEI) [22] is an X-ray radiographic technique that utilizes X-ray refraction and scatter rejection (extinction) as contrast mechanisms. It has proven to be a promising imaging method for soft tissue [23-26]. Its setup is shown in Figure 6. DEI is also a phase contrast imaging method. The feature of DEI is the use of an analyzer crystal, which is placed between the object and the detector, so it is also known as analyzer-based phase contrast imaging. The analyzer works as an angle filter. Specifically, penetrating through the object X-rays becomes scattered and with the presence of the analyzer, only those whose angles equal to the Bragg's angle can be diffracted, while others are absorbed by the analyzer crystal. Two images will be captured at the full width at half maximum (FWHM) of the rocking curve

[22]: one at the lower angle (I_L) and the other at the higher angle (I_H). Then with mathematic calculation (equation 1 & 2), apparent absorption image (I_R) and refraction angle image ($\Delta\theta_Z$) can be obtained. Apparent absorption means the combined absorption and extinction processes. Apparent absorption image (I_R) is only due to absorption contrast and has better resolution than traditional absorption image as it is scatter-free. Refraction angle image ($\Delta\theta_Z$) is only due to refractive-index contrast.

$$I_R = \frac{I_L R_H^{'} - I_H R_L^{'}}{R_L R_H^{'} - R_H R_L^{'}} \qquad (1)$$

$$\Delta\theta_Z = \frac{I_H R_L - I_L R_H}{I_L R_H^{'} - I_H R_L^{'}} \qquad (2)$$

where $R_H = R_L = \frac{1}{2}$ & $R_H' = -\frac{1}{\omega_D}$, $R_L' = \frac{1}{\omega_D}$, w_D is the Darwin width

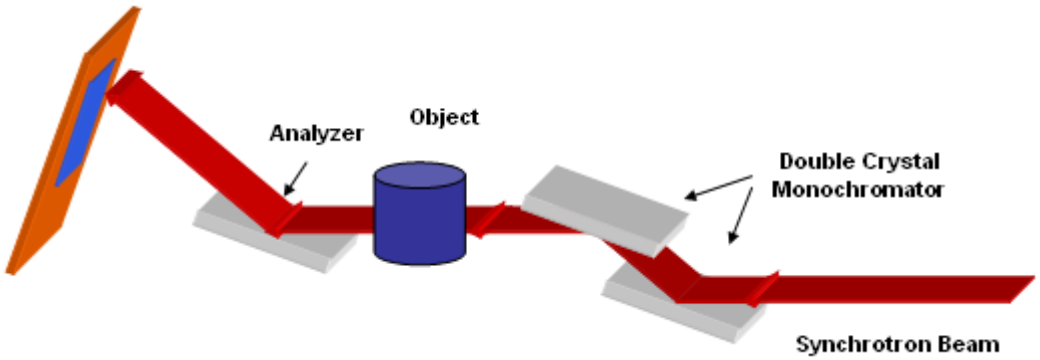

Figure 6: Schematic of diffraction-enhanced imaging (DEI) setup

Synchrotron radiation micro-computed tomography (SR μCT) utilizes the merits of synchrotron-based X-rays combined with micro-computed tomography techniques and provides three-dimensional (3D) information about the samples. The setup of SR μCT is shown in Figure 7. The arrangement of monochromators, object and detector is similar to that of in-line phase contrast imaging, except that the sample stage is rotational. Images are projected at a

certain angular step over 180 degree and then used to reconstruct by means of such algorithms as the filtered-back projection (FBP) algorithm.

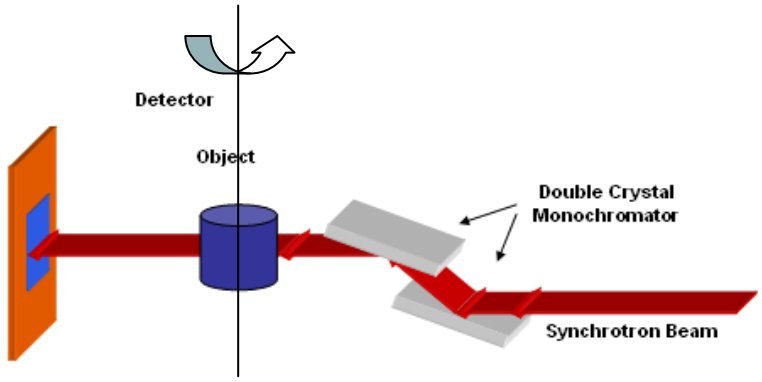

Figure 7: Schematic of SR μCT setup

1.2 Literature Review

In order to study the micro-structure of scaffold as well as the cell-scaffold interaction, many methods are applied, such as scanning electron microscope (SEM), confocal microscopy, porosimeter, light microscopy, and novel X-ray imaging method including micro-computed tomography (micro-CT) and synchrotron radiation (SR) X-ray imaging. The interaction between cells and scaffolds are widely studied in different biomaterials, such as collagen [27, 28], chitosan [29, 30], polylactic acid (PLA) [31, 32], poly-e-caprolactone (PCL) [33, 34] and alginate [35, 36]. But no research work of Schwann cell line growing from the outside and inside of alginate hydrogels, as well as in thick and thin gels, is reported.

A conventional characterization method, such as SEM, has excellent performance in showing fine surface features of biological tissues, and its spatial resolution can reach the level of sub-micro meters. Confocal microscopy, on the other hand, can focus on different layers inside a sample. However, none

of these methods can penetrate through thick samples, thus limiting them from three-dimensional (3D) evaluation and in vivo research. Also the sample preparation procedures are complex. Samples for SEM imaging are required to be sectioned and coated with high conductive material such as gold before being mounted on to sample holder. For light microscopy, samples have to be sectioned to less than 100 microns using a microtome. Samples are destroyed through these methods.

Micro-computed tomography (micro-CT) is a novel technique applied in the biomedical field and is usually applied in hard tissue imaging such as trabecular architecture in bone and skull. It is a non-destructive and non-invasive method, which means that the samples do not need to be sectioned before scanning. It can also provide three-dimensional (3D) information about the samples. Due to these merits, micro-CT has been applied to various research areas, including biomaterials and tissue engineering. In characterization of material microstructures, micro-CT has been applied to chitosan [37], poly ($_{L}$-lactic-*co*-$_{DL}$-lactide) [38], poly($_{L}$-lactic acid) (PLA) and hydroxyapatite (HA) mixtures [39] and poly caprolactone (PCL) [40] scaffolds. Until now, no research work on micro-CT analysis of micro-structure of low absorption contrast material such as alginate scaffold has been reported.

Another novel characterization method is synchrotron radiation (SR) X-ray imaging. X-ray from synchrotron radiation (SR) is a new and exciting research tool in the biomedical field. It is highly coherent and collimated, with small divergence. The X-ray beam is monochromatic. As a result, SR X-ray has higher spatial resolution and higher signal-to-noise ratio (SNR), compared to traditional X-ray imaging using the X-ray tube. It has recently been introduced as a substitute to conventional X-rays allowing high spatial resolution up to the micrometer scale and high speed imaging [41]. SR X-ray radiography has been applied in medical research area such as K-edge coronal angiography imaging

[42], tumor angiogenesis imaging without contrast agents [43], lung imaging [44], cerebellar structure imaging [45], cancer lesion [46] and so on. Mammography with SR X-ray has been carried out in clinical experiments at the SYRMEP beamline of the synchrotron radiation facility ELETTRA (Trieste, Italy) [47, 48]. The combination of structural SR transmission X-ray with functional fluorescent X-ray successfully revealed the hyperthyroidism of a human thyroid specimen, a fatty acid metabolic agent labeled rat's myocardium, and first in the world in vivo mouse brain structure [49-51]. Potentially, SR X-ray could become a very powerful tool in biological and medical applications.

Currently, the application of SR X-ray imaging in observing scaffolds is mainly limited to bone tissue engineering. Together with the computed tomography (CT) technique, synchrotron radiation micro-computed tomography (SR μCT) has been employed to observe bone scaffolds with 3-dimentional (3D) view [52-54]. Also, it is used to study human foreskin fibroblasts on polymer multifilament yarns, with the cells labeled for visualization by the use of highly absorptive agents, osmium and gold [53, 55, 56]. However, a neural scaffold, unlike a bone one that has a high attenuation index of X-ray, has an attenuation index similar to its surrounding neural tissues. This makes it hard to obtain a good contrast using traditional methods.

1.3 Objectives

The main objective of this thesis is to characterize alginate scaffolds by means of the emerging X-ray imaging techniques to study the material properties as well as biological properties. Three research objectives are to be achieved in this research, which are presented in the following, along with the methods used.

(1) Apply micro-CT imaging to characterize the structural parameters of freeze-dried alginate scaffolds including pore size, porosity, interconnectivity and wall thickness as functions of sodium alginate concentrations and freezing temperatures. Three-dimensional analysis is carried out using software (CTAn) and results are compared with scanning electron microscope (SEM) results.

(2) Study the interaction of Schwann cells with alginate hydrogels to show the proliferation of cells from outside and inside of gels, and also in thick and thin gels.

(3) Illustrate the merits of Synchrotron-based X-ray imaging techniques in low density biological samples, such as brain and muscle tissue, and alginate hydrogels. Different imaging techniques, such as absorption contrast imaging, in-line phase contrast imaging, DEI, as well as phase contrast synchrotron radiation micro-computed tomography (SR μCT) are applied to compare the merits of these imaging techniques.

1.4 Organization of Thesis

This thesis contains five main sections: Introduction, Characterization of Freeze-dried Alginate Scaffold Using Micro-CT, Characterization of Cell-cultivated Alginate Hydrogel, Synchrotron Radiation (SR) X-ray Imaging of Alginate Hydrogel, and Conclusion, Discussion and Future Work.

Included in the Introduction section are a background to the present work, a literature review of currently used characterization methods for scaffold properties, objectives, and organization of this thesis.

The next three parts are three separate but also inter-connected pieces of research work carried out during the Master's program. The first piece of research work, named Characterization of Freeze-dried Alginate Scaffold Using Micro-CT, describes the use of micro-CT for three-dimensional analysis of alginate scaffolds under different sodium alginate concentrations and freezing temperatures. Materials, methods, results, discussions and conclusions are all included.

The second piece of research work is Characterization of Cell-cultivated Alginate Hydrogel. This is a biological cell culture to study cell proliferation inside alginate hydrogels. Cells grown from outside of alginate hydrogels and inside of them are compared to determine if cells can penetrate through and move freely in gels. Also, cells cultured in thin slice of alginate hydrogels are presented to prove that the thickness of hydrogels has a great impact on cell proliferations.

The third piece is to use novel Synchrotron Radiation (SR) X-ray imaging method to study alginate hydrogel in a biological environment. Several imaging methods, such as absorption contrast and in-line phase contrast imaging, diffraction-enhanced imaging (DEI) and computed tomography (CT) techniques, are used on biological samples of alginate hydrogels enclosing rat brain tissue, as well as alginate hydrogels buried in rat muscle tissue. Photon energy effects and sample-to-detector distance effects on absorption and phase contrast imaging are illustrated.

Finally, the Conclusions, Discussion and Future Work section provides conclusions of all the work done in this thesis, explains the results obtained, and also explores ways in which the current work could be improved and expanded.

2. CHARACTERIZATION OF FREEZE-DRIED ALGINATE SCAFFOLD USING MICRO-CT

2.1 Introduction

In tissue engineering, scaffolds are usually three dimensional (3D) structures made from biomaterials that can support cell growth and conduct nutrients and growth factors so as to produce artificial organ and tissue substitutes. Therefore, scaffolds play a vital role in tissue engineering. Many biomaterials have been applied in tissue engineering, and among them, alginate is one of the most studied. Alginate is naturally derived polysaccharide that is primarily derived from seaweed. It is an ideal biomaterial for tissue engineering due to its properties that are both biocompatible and biodegradable [5, 6]. In the presence of divalent cations such as calcium ions (Ca^{2+}), alginate solution is crosslinked ionically between chains to form hydrogels [7, 8]. Scaffolds made of alginate crosslinked with calcium chloride ($CaCl_2$) can support cells and provide pores for them to penetrate through and proliferate [9].

The micro-architecture of scaffolds, based on features such as pore size, porosity, interconnectivity, and wall thickness, is of great importance in characterization of tissue engineered scaffolds. Traditional and most commonly used imaging techniques include Scanning Electron Microscopy (SEM) [53, 57]. This method gives high resolution and two-dimensional (2D) images of the surface of specimens down to the nanometer scale. Geometric features such as pore size and wall thickness can be evaluated quantitatively. A visual estimation of interconnectivity can also be achieved [58-60]. However, in order to examine the interior features of the scaffolds, physical sectioning is required, which introduces compression and edge effects to the scaffold architecture. Samples are also required to be dry and electrically conductive with a heavy metal coating. So the sample preparation procedure is quite complex and the technique yields 2D rather than 3D information.

Micro-computed tomography (micro-CT) is an increasingly common technique applied in biomedical research particularly in hard tissue imaging applications such as characterization of trabecular architecture in bone. Similar to the clinical computed tomography systems, it is a non-destructive method and provides three-dimensional (3D) information. However, for a clinical CT system, a maximum spatial resolution is usually about 1 mm^3, but for a micro-CT system, it is capable of achieving a spatial resolution of the order of 1 μm^3 [61]. Due to its merits of high resolution, non-destructive and three-dimensional analysis, micro-CT has been applied in various research areas, including biomaterials and tissue engineering. Recent use of micro-CT in scaffold research has been carried out by several groups, mostly in bone tissue engineering. The biomaterials used in bone tissue engineering, such as hydroxyapetite (HA), have relatively high X-ray absorption contrast similar to hard tissue. Alginate gel, however, has poorer absorption contrast which is a great challenge for X-ray imaging. To my knowledge, micro-CT analysis of alginate scaffolds has not yet been reported.

In this chapter, 3D porous alginate scaffolds prepared using a freeze drying technique are described. Effects of different sodium alginate concentration and freezing temperature on the scaffold microstructure are examined and evaluated. Both qualitative and quantitative results of alginate scaffolds are presented using micro-CT techniques and SEM as comparison.

2.2 Materials and Methods

2.2.1 Alginate Scaffolds

The scaffolds were made of sodium alginate (Sigma-Aldrich, USA) of different concentrations (1%, 2%, 4%, 7% weight/volume). Alginate was then crossed-linked with 1% calcium chloride ($CaCl_2$) at the volume ratio of 2:1. As both alginate and $CaCl_2$ were diluted, the final concentrations were different.

They were 2/3 of the original for alginate, and 1/3 of the original for $CaCl_2$. But for clear illustration purpose, I still use 1%, 2%, 4% and 7% alginate concentrations to state. Alginate and $CaCl_2$ solutions were put inside two syringes and pumped back and forth to make the gel [62]. Then the gel was poured into custom-made four-hole moulds (10 mm in diameter, 20 mm in height) before freeze-drying. The freeze drier was a Labconco Freezone benchtop machine. Three freezing temperatures were set: -80, -50 and -20 degrees. Samples were frozen overnight and left in the freeze drier for another 24 hours. Our original intent was to scan 10 replicates of each treatment, but scan and processing time (see below) was prohibitive. Thus, in one specimen from each treatment, 10 cylinder-shaped Volumes of Interest (VOI) of the same size (4000 microns in diameter, 1500 microns in height) were selected for analysis from each dataset.

2.2.2 Micro-CT Imaging

The scaffolds were scanned using a cone-beam high-resolution micro-CT Skyscan 1172 scanner (Skyscan, Belgium). The X-ray source was set at 60 kV of X-ray accelerating voltage and 172 μA of current. No filter was used to allow more X-rays to penetrate through and ensure higher contrast. Pixel size was 3.5 μm and exposure time is 350 ms. Approximately 2200 slices were acquired over a rotation range of 180° with a step angle of 0.2°. Small camera pixel size (4000 × 2400) was used for high resolution. Each scan took approximately 1 hour and 10 minutes. Data sets were reconstructed using standardized cone-beam reconstruction software (NRecon v1.6.1.0, SkyScan). This took approximately eight hours on a cluster of four dual-processor quad-core computers.

2.2.3 3D Analysis and Rendering

3D analysis of scanning results was carried out in CTAn (Skyscan). A standardized global threshold (22 to 255 gray levels) was used to binarize the

images into struts and background air. Despeckling was applied then to all of the VOIs to remove noise and undesired information. Structural parameters (pore size, porosity, wall thickness and closed porosity) were calculated in three dimensions from the binarized images. An automated batch analysis procedure was run on a desktop computer.

3D volume rendering of VOIs was carried out in CTVox (Skyscan) on PC.

2.2.4 Scanning Electron Microscope (SEM)

A Philips 505 Scanning Electron Microscope (SEM) at an operating voltage of 29.4 kV was used for two-dimensional scaffold imaging. Freeze-dried specimens were sectioned and sputter gold coated before mounted onto a sample stage.

2.3 Results

The novel micro-CT imaging technique was used to obtain internal structural information about 3D alginate scaffolds without sectioning and damaging samples. On this basis, the effects of alginate concentration and freezing temperature on scaffolds parameters, such as pore size, porosity, wall thickness and interconnectivity, were examined and characterized.

2.3.1 Alginate Concentration Effects on Scaffolds

2.3.1.1 Qualitative Observations

Firstly, the effects of sodium alginate concentrations (7%, 4%, 2% and 1% w/v) on microstructure of scaffolds were investigated, when keeping the freezing temperature the same (i.e., -80 ^{o}C). Micro-CT cross-sectional images (Figure 8 a, c, e, g) and 3D volume rendering results (Figure 8b, d, f, h) provide qualitative appreciation of scaffold structure. Pore size and porosity becomes smaller with higher alginate concentration. Also, at lower concentration, an isotropic pore structure is more obvious, while at higher concentration, an anisotropic lamellar plate-like structure predominates. The 3D models in

Figure 8 show one of the volumes of interest (VOI) from the corresponding samples. The 2D Micro-CT cross-sectional images are the first layers from the 3D models.

SEM images of the sectioned surface of alginate scaffolds provide similar results (Figure 9). Pore size decreased with higher alginate concentrations. Also, with higher alginate concentrations, such as 4% and 7%, preferentially oriented structure indicating the ice growth direction in horizontal cross-section can be observed. On the other hand, with lower alginate concentrations, such as 1% and 2%, isotropic structure is shown. These features are in accordance with those observed from Figure 8.

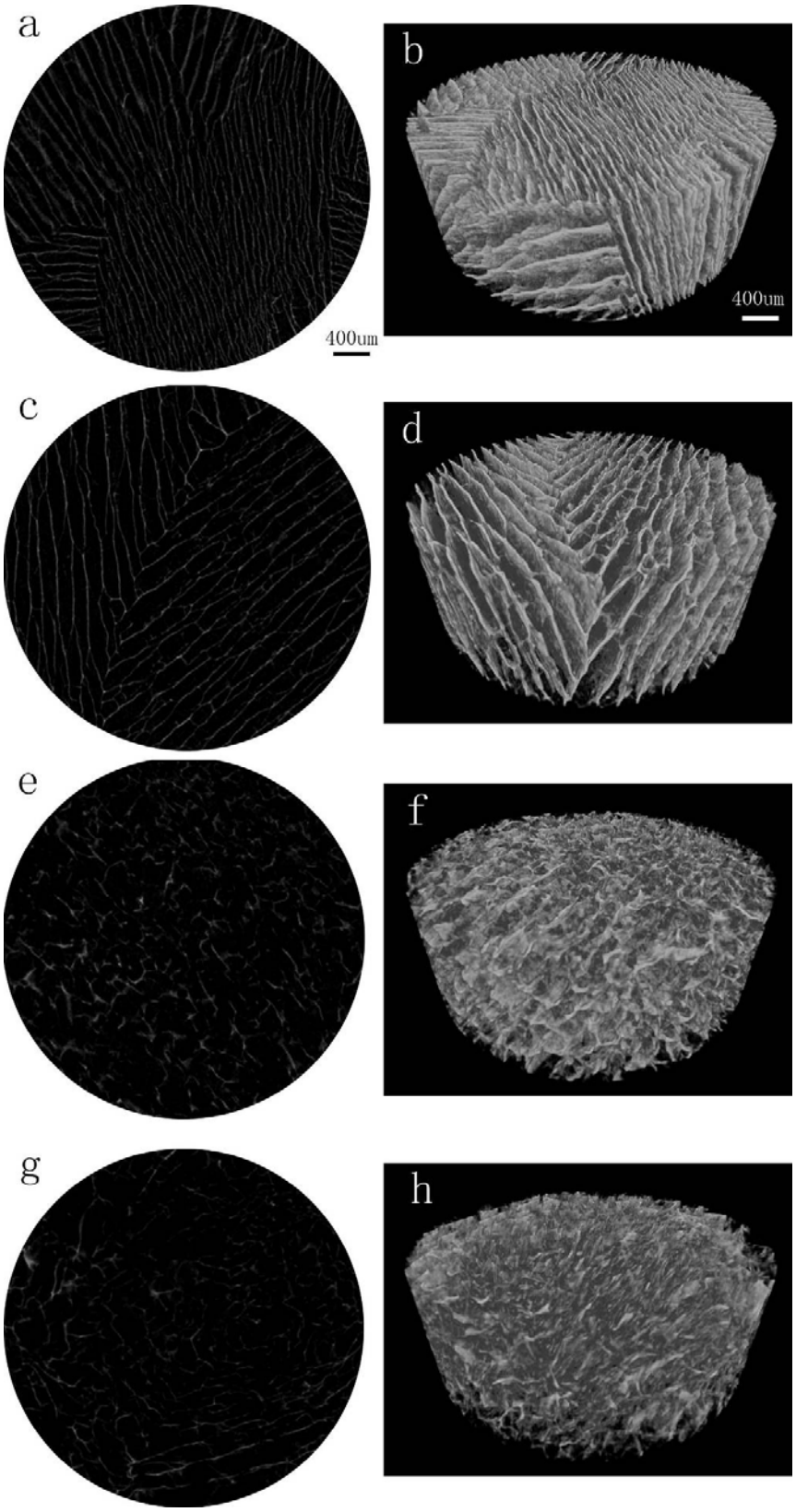

Figure 8: Micro-CT cross-sectional images of 7% (a), 4% (c), 2% (e) and 1% (g) alginate solutions. Figure 8(b), (d), (f) and (h) show the three-dimensional rendering of the corresponding 7%, 4%, 2% and 1% alginate scaffolds.

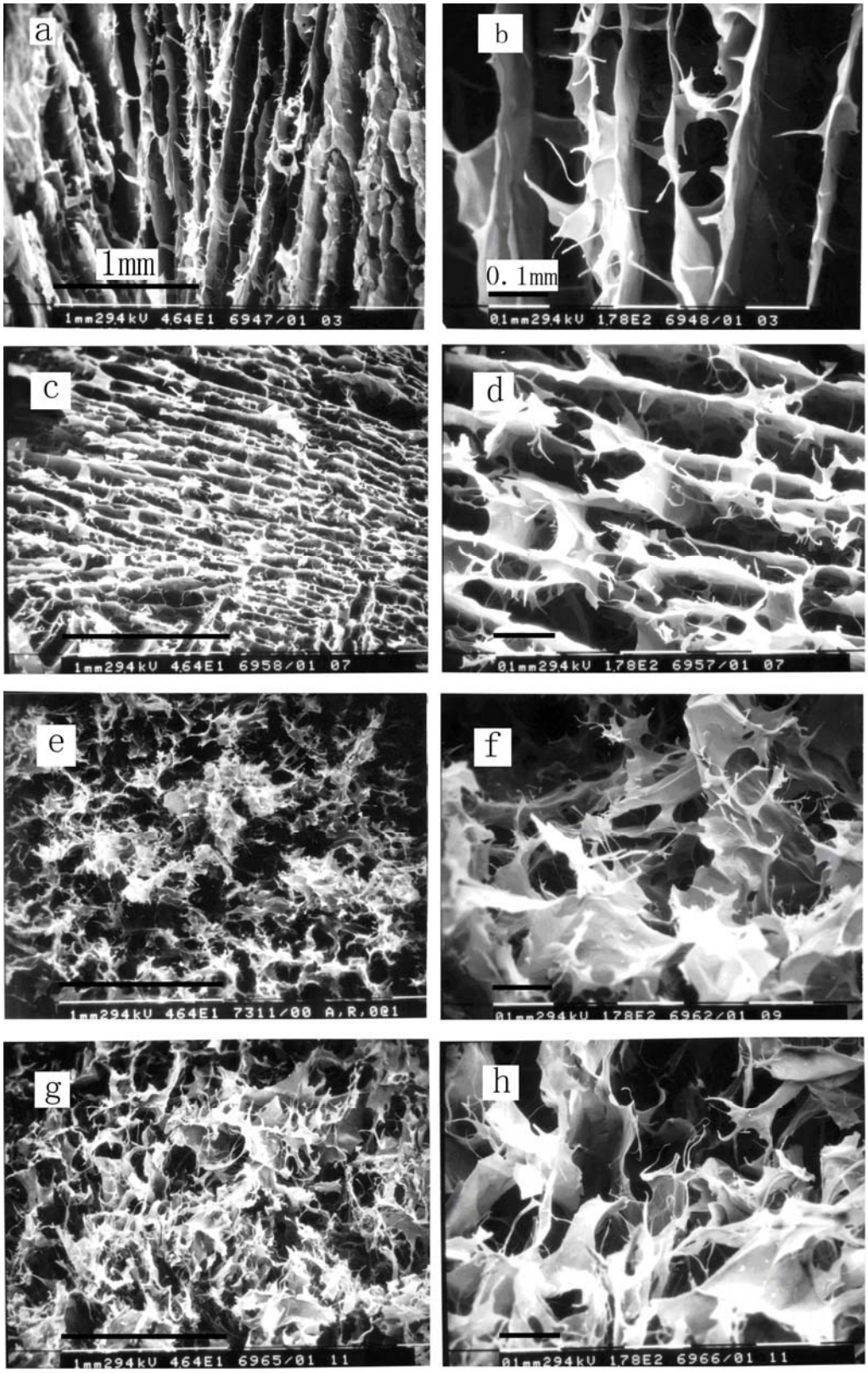

Figure 9: SEM of alginate scaffolds at 7% (a), 4%(c), 2%(e) and 1%(g) of solution concentration (×46.4). Figure 9(b), (d), (f) and (h) are corresponding magnified images (×178).

2.3.1.2 3D Quantitative Analysis of Porosity and Pore Size

From 3D analysis results of micro-CT data using CTAn, it can be seen that at the same freezing temperature, lower alginate concentration tends to have higher porosity (Figure 10). In linear regression test (SPSS V.17.0), $p<0.001$, indicating that the relationship between porosity and alginate concentration is statistically significant. The increments of porosity are similar with decreased alginate concentrations. On the other hand, with higher alginate concentrations, smaller pore sizes were observed ($p<0.001$, linear regression test) (Figure 11). The 3D quantitative analysis results provide strong support of what is observed qualitatively above. Error bars in figures represent the standard deviation of data.

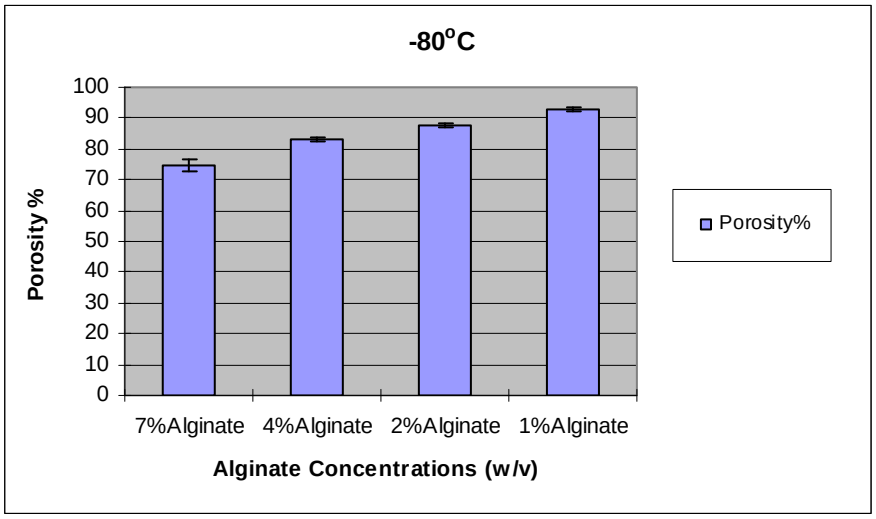

Figure 10: Changes of porosity with different alginate concentrations (1%, 2%, 4%, 7%) at -80 ^{o}C.

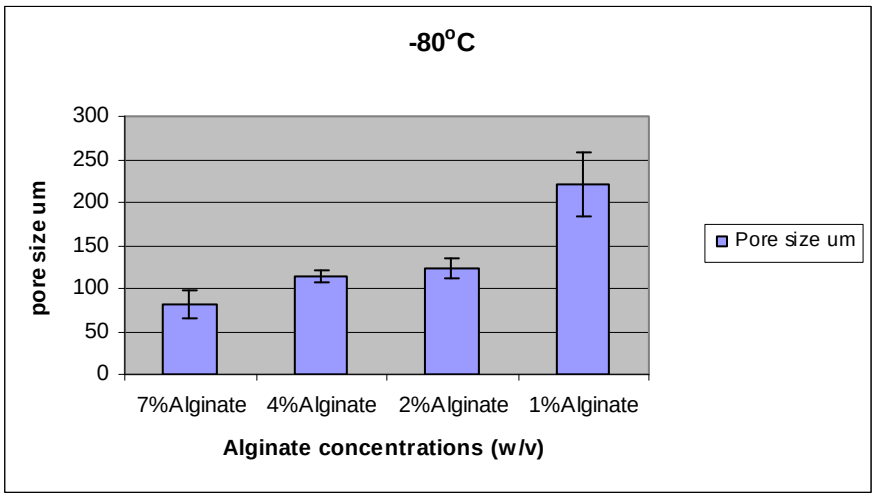

Figure 11: Changes of pore size with different alginate concentrations (1%, 2%, 4%, 7%) at -80 ^{o}C.

2.3.2 Freezing Temperature Effects on Scaffolds

2.3.2.1 Qualitative Observations

While keeping alginate concentration fixed (7% w/v), the effects of freezing temperature on scaffolds was examined. Micro-CT cross-sectional images and 3D volume rendering results of alginate scaffolds frozen to -80 ^{o}C, -50 ^{o}C and -20 ^{o}C are shown in Figure 12. Pore size becomes smaller with the use of lower freezing temperature and also plate-like structures becomes more obvious.

SEM images given in Figure 13 show the geometrical observations of the scaffolds. These images suggest that with higher freezing temperature, isotropic structure is more obvious, which provides further support to what is observed in Figure 12.

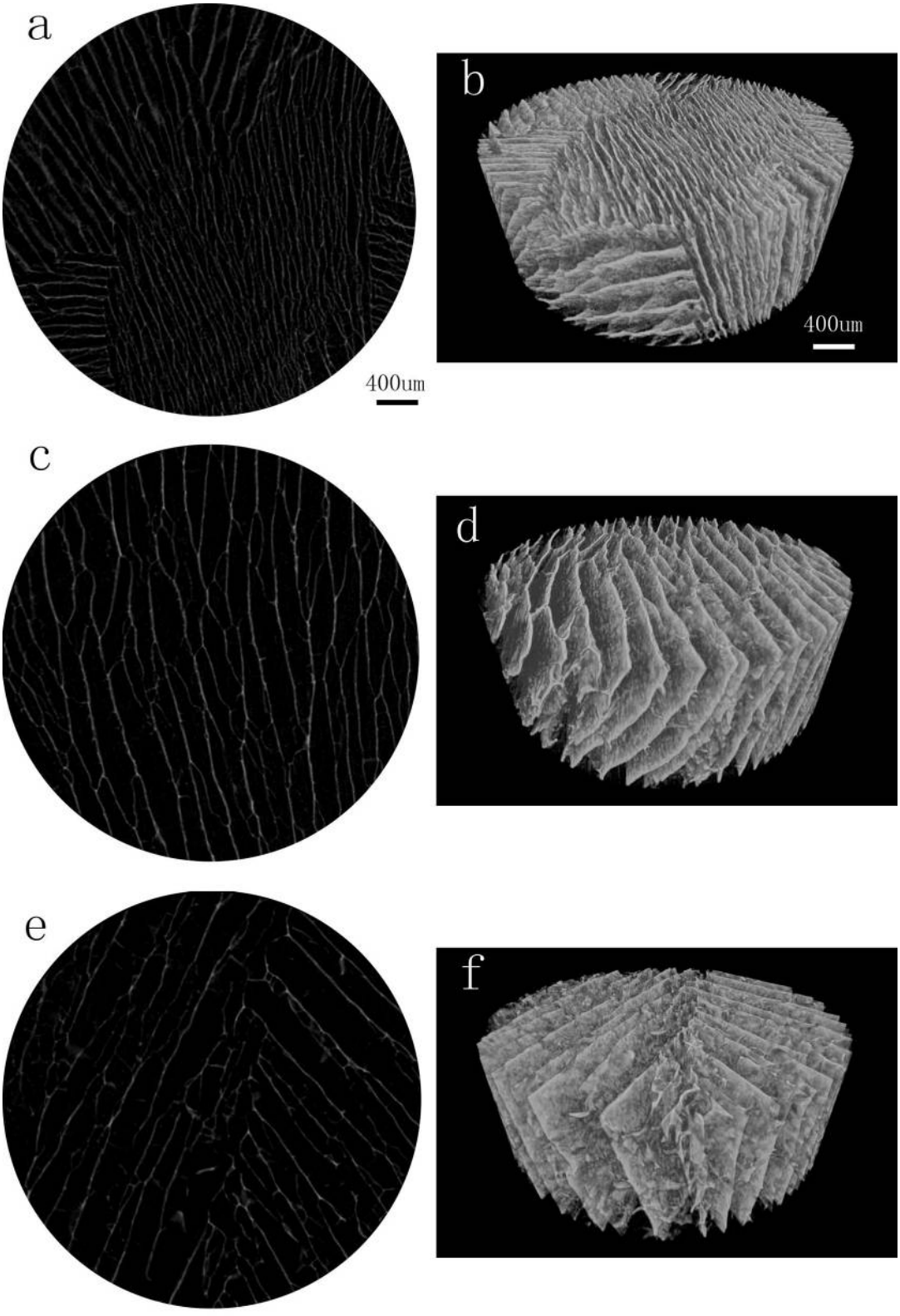

Figure 12: Micro-CT cross-sectional images of scaffolds made with 7% alginate solution and frozen to -80 ^{o}C (a), -50 ^{o}C (c) and -20 ^{o}C (e). Figure 12(b), (d) and (f) are 3D volume rendering of alginate scaffolds frozen to -80 ^{o}C, -50 ^{o}C and -20 ^{o}C respectively.

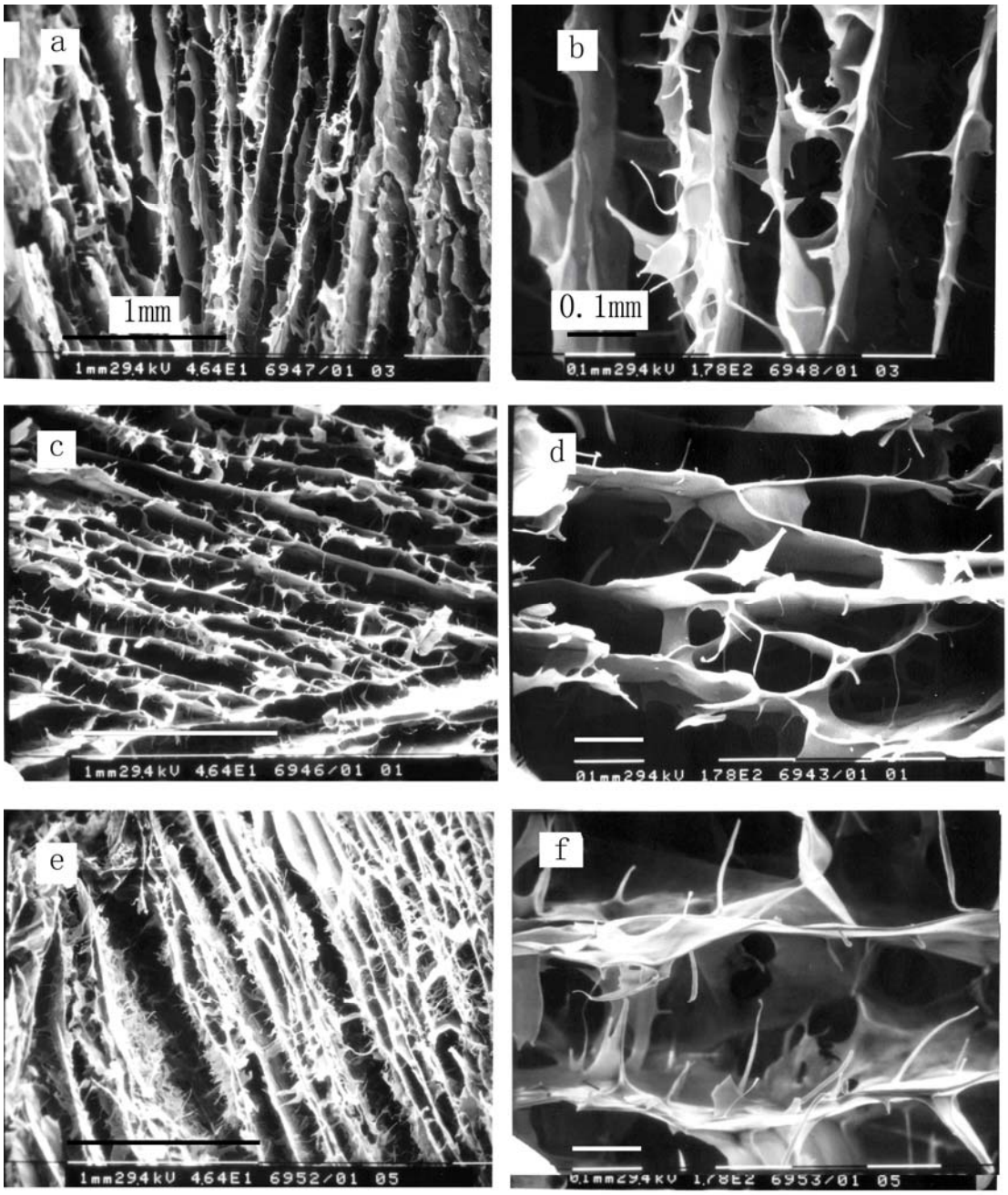

Figure 13: SEM of alginate scaffolds at -80 ^{o}C (a), -50 ^{o}C (c) and -20 ^{o}C (e) of freezing temperature (×46.4). Figure 13(b), (d) and (f) are corresponding higher magnification images (×178).

2.3.2.2 3D Quantitative Analysis of Porosity and Pore Size

From 3D analysis results of micro-CT data, it can be seen that at the same alginate concentration, lower freezing temperature resulted in smaller pore size ($p<0.001$, linear regression test) (Figure 14) . As to the porosity, lower freezing

temperature tends to result in smaller porosity (Figure 15). These quantitative results are in accordance with morphological observations from micro-CT and SEM above. Error bars in figures represent the standard deviation of data.

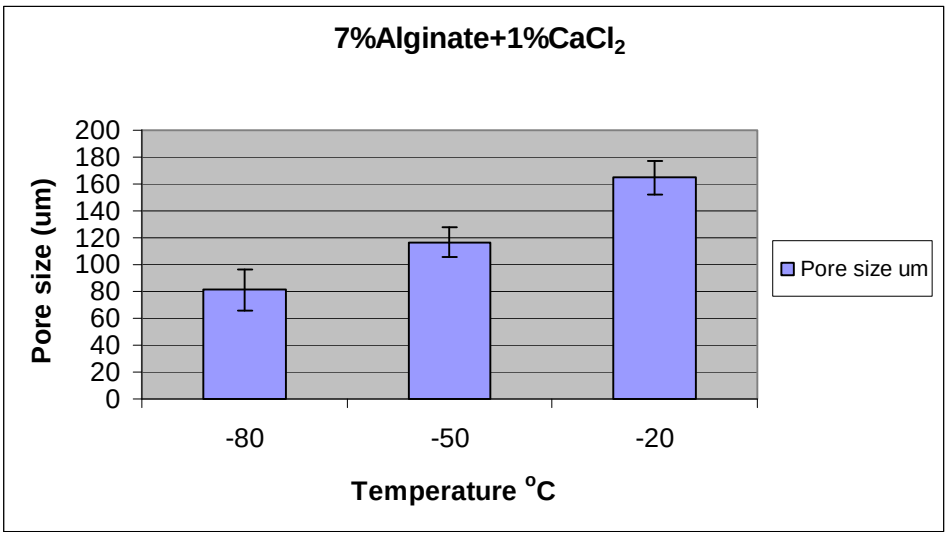

Figure 14: Changes of pore size with different freezing temperature of 7% alginate concentration.

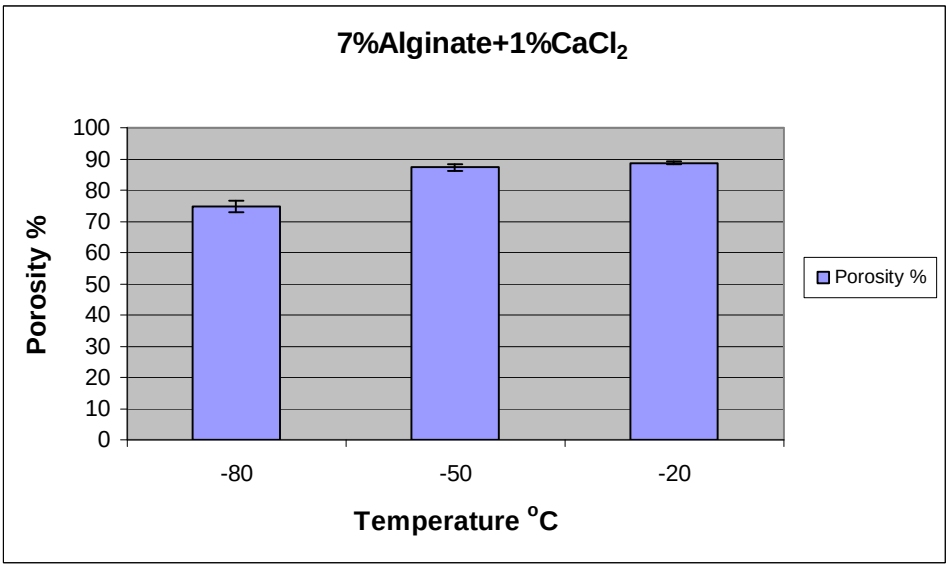

Figure 15: Changes of different porosity of scaffolds made with 7% alginate solution.

2.3.3 Interconnectivity and Wall Thickness

Interconnectivity is another important parameter in the characterization of

porous scaffolds, which is measured by means of closed porosity. Closed porosity is the percentage of pores that are not inter-connected, thus ‘closed’. The smaller the closed porosity, the better the interconnectivity is.

A highly interconnected scaffold can provide a supportive space and interlink for cells to grow. Table 1 demonstrates that the closed porosity of the alginate scaffolds is almost 0 regardless of alginate concentration or freezing temperature. That is to say, scaffolds made with alginate have excellent interconnectivity.

Also for wall thickness, no significant differences are found to associate with alginate concentrations or freezing temperatures (Table 1).

In a linear regression test, given the same alginate concentration (7%), the p-value for comparing different freezing temperatures (-80, -50, -20) and wall thickness is 0.174, larger than 0.05. Therefore, freezing temperature has no relationship with wall thickness. Given the same freezing temperature (-80), the p-value for comparing different alginate concentrations (7%, 4%, 2%, 1%) and wall thickness is 0.259>0.05. So alginate concentrations have no relationship with thickness. That is to say, wall thickness is independent of alginate concentrations and freezing temperatures.

Table 1: Measured closed porosity and wall thickness of alginate scaffolds.

	Closed Porosity %:	Wall Thickness um:
7% Alginate+1% $CaCl_2$ -80	0.00418±5.14E-06	26.57±4.26
4% Alginate+1% $CaCl_2$ -80	0.00224±7.4E-06	24.60±0.66
2% Alginate+1% $CaCl_2$ -80	0.00102±3.35E-07	26.09±2.65
1% Alginate+1% $CaCl_2$ -80	0.00116±1.19E-07	25.41±1.02
7% Alginate+1% $CaCl_2$ -50	0.00081±6.44E-08	21.00±0.65
7% Alginate+1% $CaCl_2$ -20	0.00084±1.06E-06	24.91±0.43

2.4 Discussions

Hydroxyapatite (HA), an osteophilic ceramic related to the inorganic component of bone [59], is a good substitute material in bone tissue engineering. It has good X-ray absorption contrast, thus facilitating micro-CT imaging. Turco et. al. [7] have conducted micro-CT analysis of alginate/hydroxyapatite scaffolds in bone tissue engineering. However, in nerve tissue engineering, biomaterials used to build scaffolds are required to have excellent biodegradability. Alginate is ideal for nerve tissue engineering but presents a big challenge for micro-CT imaging as it has poor X-ray absorption contrast as soft tissue does. The current results in this research work suggest that micro-CT does have the potential to characterize low-contrast biomaterials with X-ray imaging.

The micro-architecture of scaffolds, such as pore size and porosity, is of great importance, as it affects not only cell survival, signaling, growth, propagation and reorganization, but also plays a major role in cell shape modeling. Scaffolds must possess an open-pore (interconnected) internal structure with a highly porous surface and microstructure that allows cell in-growth and reorganization in vitro and provides the necessary space for neovascularization from surrounding tissues in vivo. The optimal porosities are greater than 90% depending on different applications [63, 64]. The required pore sizes vary from one cell type to another. For example, pore sizes ranging from 200 to 400 um are optimal for bone tissue engineering [65, 66], 20 to 125 um for adult mammalian skin [67] and 45-150 um for regenerating liver tissues [68]. In this study, we have the pore size of alginate scaffold ranging from 80 to 220 um and porosity from 75% to 93%. These data show that alginate scaffolds made with freeze-drying technique are suitable for the aforementioned applications.

2.5 Conclusions

This part of thesis introduced the micro-CT imaging to characterize, both qualitatively and quantitatively, low-contrast alginate scaffolds. The micro-architecture of the scaffolds, such as pore size, porosity, interconnectivity

and wall thickness was evaluated and characterized. It is concluded that lower freezing temperature and higher alginate concentration lead to smaller pore size, while higher freezing temperature and lower alginate concentration result in higher porosity. Also, the images obtained show the fabricated alginate scaffolds have good interconnectivity for cells to grow.

3. CHARACTERIZATION OF CELL-CULTIVATED ALGINATE HYDROGEL

3.1 Introduction

Currently, many research groups encapsulated cells inside scaffolds to provide a three-dimensional structure for cells to proliferate and form new tissue. As alginate is a natural biomaterial, with good biocompatibility and biodegradability, the interaction of alginate with cells is of great interest.

Schwann cells are a glial cell type of peripheral nervous system (PNS). They wrap around the axon to form the myelin sheath. They are also capable of re-organizing the glial scar, which could promote greater axonal regeneration. Schwann cells are critical for recovery from peripheral nerve injury (PNI).

In this chapter, the interactions of alginate hydrogel with Schwann cells are studied. It is of great interest to discover if cells are able to grow and divide inside the hydrogel scaffolds. Anther question to be answered is whether if cells, cultured outside hydrogel scaffolds, can penetrate into the interior of scaffolds.

3.2 Materials and Methods

3.2.1 Cell-cultivated Scaffolds Preparation

A rat Schwann cell line (RSC96, ATCC) was grown in Dulbecco's Modified Eagle Medium (DMEM) with 10% fetal bovine serum (FBS) in a 37 ^{o}C and 5% CO_2 incubator. Cultures were treated with 0.1% trypsin at 37 ^{o}C for 5 minutes to detach them from the culture dish. Then cells were blended with 4% sterile sodium alginate solution (Sigma, USA) and diluted to a density of 1×10^{6}/mL. Cell-blended alginate solution was poured into the lower half of custom-made cylinder-shaped moulds. The mould has four holes, and each has a diameter of 1 cm and a height of 2 cm. Then 2% calcium chloride ($CaCl_2$) was added on top into the four holes to crosslink with cell-blended alginate solution and form

cylinder-shaped cell-cultivated alginate hydrogels. Each gel was around 1 cm in diameter and 0.5 cm in height. Four replicates were made for each group and cultured for 1 and 4 days respectively. As comparison to cell growing inside gels and growing from outside, a third group was obtained by making alginate gels first (without blending with cells) with similar procedures described above, which were then moved to 6-well plate. Cells diluted with Dulbecco's Modified Eagle Medium (DMEM) were added and seeded on the surface of the gels to see if cells could penetrate through and grow into gels. The third groups were cultured for 4 days. One control group was made with 4% sodium alginate crosslinked with 2% $CaCl_2$ without cell seeding.

In order to compare cells cultured in thick cylinder-shaped gels and thin slices, the Schwann cell line (10×10^6/mL) was used to firstly make four cylinder-shaped alginate gels as mentioned previously. Then one cell-cultivated alginate hydrogel was cut into four 100-micron slices with cells still alive on day 0 and then put into incubator for continued culturing. This was done under a sterile environment to ensure cells were not contaminated during the sectioning. There may have been some cell death near the blade surface during sectioning, but most of them were still alive inside the 100-micron slice. Both the thick gels and thin slices were cultured for 4 days and 8 days, respectively, before fixing and staining.

3.2.2 Cell Fixing and Staining

4% Para-formaldehyde (PF) made with 10 mM Tris buffer and 2% $CaCl_2$ solution was used to fix the alginate hydrogels. Calcium ions (Ca^{2+}) were added to the 4% PF solution so that the alginate hydrogels stayed in an environment surrounded by Ca^{2+} and would not fall apart. This 4% PF could not be made with phosphate buffer solution (PBS) as phosphate ions would react with calcium ions and form calcium phosphate precipitate. 10 mM Tris buffer was diluted from 1M Tris stock solution made with Trizma Base (Sigma, USA). A

pH meter was used to monitor the pH value of Tris buffer to 7.4. To make 100 mL 4% PF solution, 4 g para-formaldehyde powder (Sigma, USA), 2 g calcium chloride (Sigma, USA), 0.94 mL 1M Tris block solution and 93.06 mL distilled water were needed. Firstly, distilled water was heated to 60 ^{o}C. Next, 4 g para-formaldehyde powder was added and stirred. The solution would become cloudy. One to two drops of concentrated NaOH solution were added until the PF solution was clear. Then, 0.94 mL 1M Tris stock solution was added along with 2 g calcium chloride powder and stirred. When the solution was cooled down, it was labeled and stored at 4 ^{o}C.

Once the medium were soaked into the gels, 4% PF was added into each well and placed in a cold room with a temperature of 4 ^{o}C for 24 hours. Then, the gels were washed in 10 mM Tris buffer with 2% $CaCl_2$ solution for 2 hours with the purpose of removing the PF solution left inside the gels. Here, the 10mM Tris buffer was also made with 2% $CaCl_2$ to ensure the gels were staying in a calcium ion environment so that they would not fall apart.

In order to visualize cells under light microscopy, a histological staining method using Cresyl Violet Stain was applied. Stock solution was made with 0.5% cresyl violet dissolved in 20% ethanol, and stored at 4 ^{o}C. Working solution was made by filtering 300 mL stock solution and then adding 5 mL glacial acetic acid. After sectioned samples were collected on gelatin subbed slides, they were put in air to dry for around 30 minutes. Then, slides were put in cresyl violet solution for 4 min followed by distilled water for 2 min. After that, slides were moved through a gradient of ethanol, i.e. 50% ethanol for 2 min, 70% Ethanol with one drop of concentrated Acetic Acid for 2 min, 90% ethanol for 2 min, 95% ethanol for 2 min, 100% ethanol for 4 min and 100% ethanol for 4 min for thorough dehydration. Finally, slides were soaked in two tanks of xylene, each for 10 min, before being mounted with the permanent mounting medium Permount.

3.2.3 Light Microscopy

Light microscopy is a traditional and widely-used method to visualize cells. Here, it was used as a supporting method to see the details inside alginate hydrogels. Before taking pictures using light microscopy, the gels were fixed with 4% PF solutions and then sectioned with vibratome (Leica VT1200). The slices were 100 microns thick and all pencil-labeled on the frosted end of slides. Then the slides were stained with Cresyl Violet Stain as described above, and imaged with Zeiss light microscopy (Zeiss Imager M1).

3.3 Results

3.3.1 Comparison of Gels Blended With Cells and Without Cells

In order to compare the growth of the cells that were blended inside alginate hydrogels to the growth of the cells that were placed outside the hydrogel, both hydrogels were cultured for 4 days. The results obtained from light microscopy are shown in Figure 16. Figures 16(a) and (b) are alginate gel slices without cells blended inside. It can be seen that there are almost no Schwann cells inside the gels after 4 days culture, suggesting that Schwann cells cannot grow into alginate hydrogels as they can go into other porous biomaterials such as PCL [69]. The reason is mainly due to the fact that alginate gel, once formed, has pores that are too small for cells to move inside. On the contrary, when cells were blended with alginate solutions before hydrogel formation, they can be seen clearly inside (Figures 16c and d). Cresyl Violet stained the nuclei. Cells are evenly distributed, which means they were blended evenly inside alginate solutions. The size of an individual cell is around 2-3 microns.

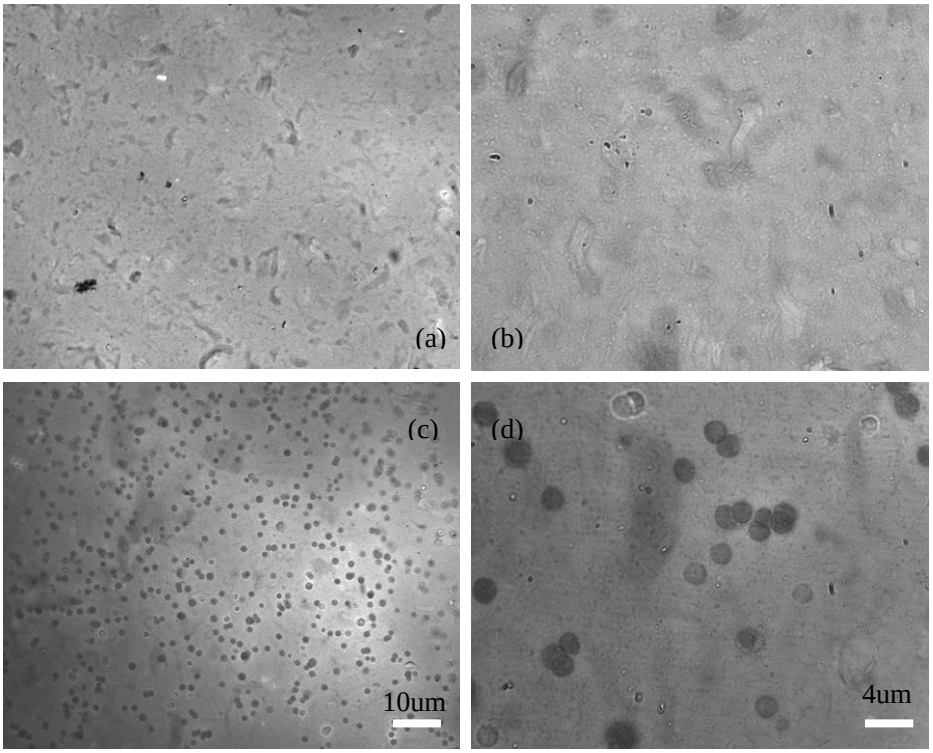

Figure 16: (a) and (b) are 10X and 40X microscope images of alginate gels without cells blended, once cultured for 4 days; (c) and (d) are 10X and 40X microscope images of cell-blended alginate gels, once cultured for 4 days.

3.3.2 Cell Growth inside Gels

3.3.2.1 Cell Growth in 1 Day and 4 Days

For cell-blended hydrogels, the cell growth, once cultured for 1 day and 4 days, was examined. The Schwann cell line (1×10^6/mL) was blended with alginate solution, and made into cylinder-shaped gels. Gels were cultured for 1 day and 4 days respectively. Figure 17 shows the light microscopy of cells grown in alginate gels. Figure 17(a) is cell-cultivated gel in 1 day and Figure 17(b) in 4 days. After cultured for 4 days, more cells can be observed inside. Figure 17(a) contains 79 cells and Figure 17(b) has 132 cells in the same area of 2064 square microns. Also, cell division is more obvious in the 4-day samples, which means cells can survive and propagate inside alginate gels.

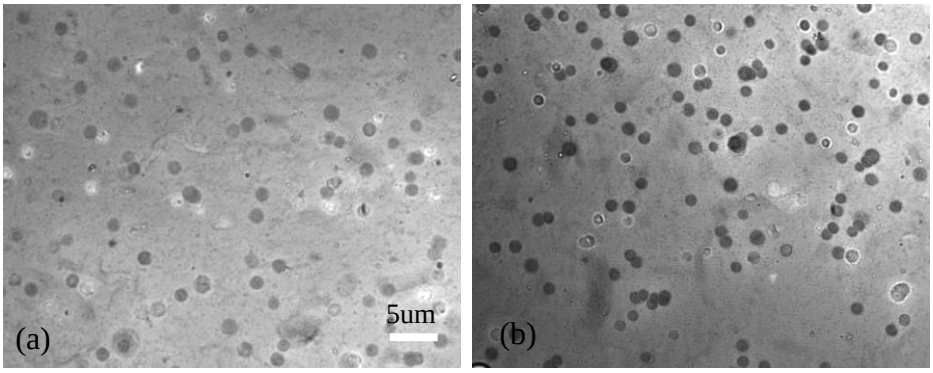

Figure 17: Microscopy results of cell-cultivated alginate gels that were cultured for 1 day (a) and 4 days (b).

3.3.2.2 Cell Growth in Thick and Thin Gels

The Schwann cell line (10×10^6/mL) was prepared to make cell-cultivated alginate gels in order to compare cell growth in thick and thin gels. For the first group, cell-cultivated alginate hydrogels were made with a cylinder shape of 10 mm in diameter and 10 mm in height. For the second group, gels were cut, with cell still alive, into 100 micron slices using a vibratome. Both groups were then placed into an incubator and cultured for 8 days.

Figure 18 shows the results of both groups in light microscopy. Cells grown in thin slices (100 micron) (shown in Figure 18b) have larger diameter than those grown inside thick cylinder-shape gels (Figure 18a). The average cell diameter in Figure 18(b) is 1.93 microns while that in Figure 18(a) is 1.49 microns. Also, cells tend to divide and cluster in thin gels. As shown in Figure 18(c), which is the enlarged image of part of Figure 18(b), newly grown cells are observed in clusters.

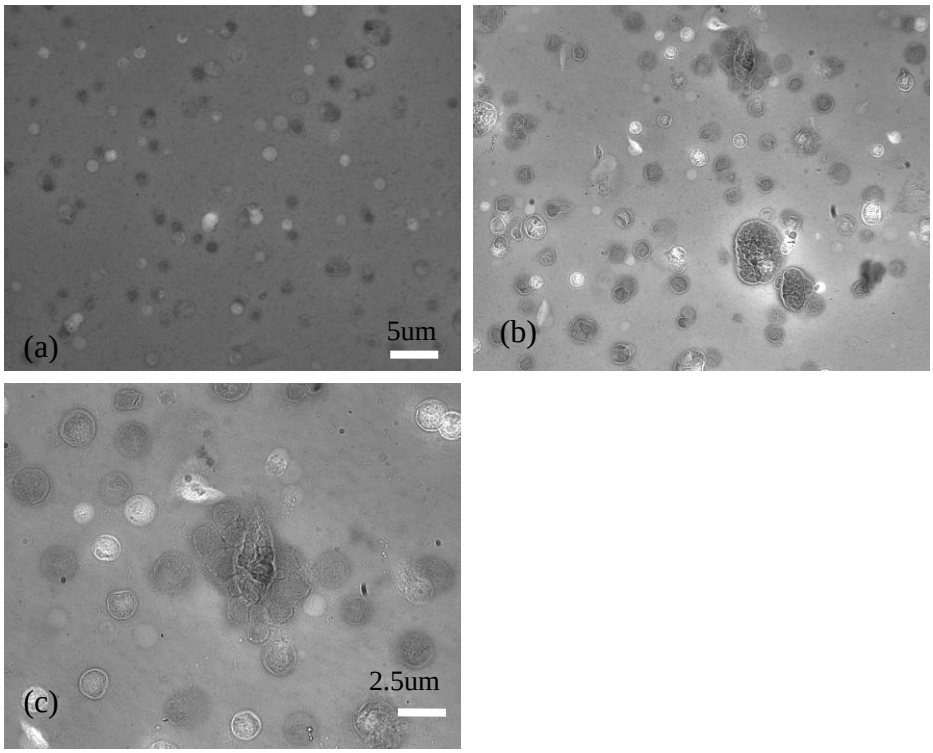

Figure 18: (a) and (b) are 20X microscopy images of cell-cultivated alginate gels. Figure 18(a) shows cells cultured in thick cylinder-shape gel and (b) shows cells in thin gel slice. Figure 18(c) is 40X microscopy image which reveals the enlarged part of clustered cells in Figure 18(b).

What is more interesting is that clusters of cells with the shape and extended morphology similar to those cultured in pure medium can be observed in thin alginate gels (Figure 19). It can be concluded that cells grown inside thick gels are mostly round in shape and do not stretch out. Even when they divided, they remained in round shape. However, when cultured in thin gels, cells could proliferate more and stretch to the surrounding as a rod shape, similar to when they are cultured in medium. Large clustered cells can be observed with a diameter of about 34 microns. The reason for cells to proliferate and divide more freely in thin gels is mainly due to the fact that DMEM and other nutrients outside can penetrate into thin slices more easily, resulting in better transfer of nutrients and cell waste.

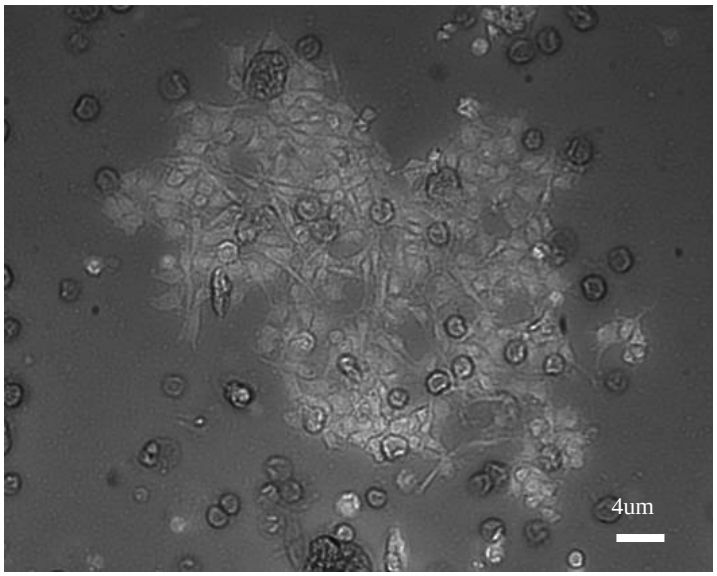

Figure 19: Microscopy image of cells cultured in thin alginate gel for 8 days. Large cluster of cells which were divided and stretched can be observed.

3.4 Discussions and Conclusions

From this work, some conclusions can be drawn on cell proliferations inside alginate gels and from outside into gels. As alginate hydrogels were thick and solid, with pores smaller than cell size, cells could hardly grow into gels from outside. Inside thick gels, cells would survive and divide as the culture days increased, but they tended to stay in round shape and not be able to stretch around and cluster. Difficulties in penetration into thick gels result in limited medium and nutrients transferring with cell wastes, which prevent cells from stretching out and growing in size. On the other side, when cultured in thin slice of alginate gels (100 microns in this experiment) cells were more able to proliferate and stretch towards the surroundings as they did in medium solutions. They appeared to have a rod shape rather than a round one. Also, the size of cells was larger than that in thick gels.

In most of these experiments, gels were soaked in a 2% Ca^{2+} environment to prevent the gels from swelling and falling apart, except for cell culturing. During cell culture, no additional 2% calcium ions were added because the high

concentration of calcium ions would destroy the potential balance inside and outside of cell membrane, resulting in killing the cells. DMEM already contains small amount of calcium ions for cells to survive. These calcium ions even at a lower concentration apparently helped to maintain the alginate hydrogels in good cylinder shape after culture for 8 days.

In these experiments, 4% sodium alginate solution and 2% calcium chloride solution were used for the study of cell-biomaterial interaction. Other concentrations of sodium alginate and calcium chloride may be used in the future. However, when 4% sodium alginate was crosslinked with 2% $CaCl_2$, a solid hydrogel was formed which could also be used for synchrotron radiation X-ray imaging described in the next chapter. On the contrary, when lower concentrations of alginate and $CaCl_2$ were crosslinked, the resulting hydrogel was not as good in maintaining a cylinder shape compared to the experiments presented in this chapter.

4. SYNCHROTRON RADIATION X-RAY IMAGING OF ALGINATE HYDROGEL

4.1 Introduction

X-ray imaging of biological samples has become quite popular due to its easy sample preparation and non-destructive and non-invasive properties. Apart from clinical use, X-ray imaging has also been used in research of biomaterials and tissue engineering. The problem facing biomedical imaging, however, is the similar absorption properties of X-rays among soft tissues. Soft tissues, for example, lung tissue and brain tissue, have similar absorption contrast and are very close in density with lesions. As such, they are difficult to distinguish in an image. X-ray absorption of hydrogels is similar to that of soft tissues. For traditional X-ray imaging using tube X-ray, absorption contrast is the main contrast to distinguish among different features inside the sample. When X-ray penetrates through samples, it will be absorbed and attenuated. The attenuation coefficient is a property of materials. As both soft tissues and hydrogels mainly consist of water, the attenuation coefficients among them are similar, resulting in similar attenuated X-rays. Therefore, the differences at the edge of features are hard to resolve. Thus, samples of similar density and attenuation coefficient are rarely distinguishable in traditional X-ray imaging.

Apart from absorption contrast, the phase contrast imaging technique is growing in popularity. Different from absorption imaging which utilizes different absorption attenuation coefficient, phase contrast is in favor of X-ray refraction when penetrating through an object. The major difference between absorption contrast and phase contrast imaging lies in the distance between sample and the detector, as shown in Figure 5. In absorption imaging, the detector is placed right behind the sample to collect attenuated X-rays; while in phase contrast imaging, the detector is placed tens of centimeters to a few meters away from the sample to collect refracted X-rays. With longer distance after going through the sample, the

X-ray refraction effects become more obvious. The bending at the edge of different features inside a sample results in the pitch in the gray value plot, which gives better contrast. Due to the fact that X-rays are travelling further before hitting the detector, the attenuation and scattering in the atmosphere is more intense, which requires a purer, monochromatic X-ray source with even higher photon energy. X-rays coming from a traditional X-ray tube cannot meet these requirements.

With the development of the synchrotron radiation (SR) facility, X-ray imaging using phase contrast and other techniques becomes possible. Synchrotron radiation (SR) is the phenomenon of radiation which occurs when charged particles are accelerated in a curved path or orbit. It has a wide energy range from infra-red to hard X-rays. SR X-ray imaging is a new and exciting research tool in the biomedical field. It is highly coherent and collimated with small divergence. The X-ray beam can be selected to be monochromatic. As a result, SR X-ray has higher spatial resolution and higher signal-to-noise ratio (SNR), compared to traditional tube X-ray. It has recently been introduced as a substitute to conventional X-rays allowing high spatial resolution up to the micrometer scale and high speed imaging. Synchrotron-based absorption imaging, in-line phase contrast imaging and diffraction-enhanced imaging (DEI) are heated research methods. Also, combined with micro-computed tomography (micro-CT), synchrotron radiation micro-computed tomography (SRμCT) is performed to provide three-dimensional (3D) visualization as well as analysis of samples.

In this chapter, high energy and monochromatic X-rays from the Canadian Light Source (CLS) synchrotron facility was used to visualize rat brain tissue inside alginate hydrogels as well as cell-cultivated alginate hydrogels buried in rat muscle tissue. Absorption and in-line phase contrast were performed as a comparison using different photon energies and different sample-to-detector (SD)

distance. DEI and SR μCT were also carried out. Heavy metal staining of osmium tetroxide (OsO_4) was used as a comparison to samples without any staining.

4.2 Materials and Methods

4.2.1 Alginate Gels Made with Brain Tissue

Rat brain tissue, obtained from a healthy rat, was sectioned into several 200 micron slices using a vibratome. Sliced brain tissue was then placed inside 4% alginate solution and covered with 2% $CaCl_2$ for crosslinking. The brain tissue stayed in the middle of the alginate after gelation. One of the hydrogels with brain tissue inside was stained with 0.1% osmium tetroxide (OsO_4) as a comparison to those without staining. Figure 20 shows two examples of brain tissue embedded in alginate hydrogels. The left one appears darker due to OsO_4 staining. The right one is the hydrogel without any staining.

Figure 20: Alginate hydrogels made with brain tissue inside. The left one is stained with OsO_4 and appears darker than the right one, which is without any staining.

Osmium tetroxide (OsO_4) is one of the most common contrast stains for X-ray imaging of soft tissues, and it is a natural candidate. Osmium has electron binding energies favorable for strong X-ray absorption, and is known to bind to cell membranes and other lipid-rich structures including nerves. When stained

with osmium, samples will turn black. Alginate hydrogel with brain tissue embedded was soaked in 0.1% OsO_4 for 24 hours and then washed with 10 mM Tris buffer with 2% $CaCl_2$ solution for another 24 hours. For better permeation of solutions into hydrogels, samples were placed on a stirrer located in a cold room.

4.2.2 Cell-cultivated Alginate Gels Buried in Rat Muscle Tissue

Rat muscle tissue was obtained from a healthy rat leg muscle and was cut into a thin slice (100 microns). Cell-cultivated alginate hydrogel (4 days, 10×10^6/mL) obtained from previous experiment was stained with 0.5% OsO_4 and covered nicely by the thin layer of rat muscle tissue. Figure 21 shows the cell-cultivated alginate hydrogel covered by thin layer of rat muscle tissue. In the middle of the sample, the black part is noticed due to the fact that the alginate hydrogel was stained with OsO_4. The sample was put in a square-shaped tube mounted with plastic foam. Plastic foam has very low X-ray absorption, so is good as a mounting material. The sample tube was then used for imaging by means of X-ray beamline.

Figure 21: OsO_4 stained cell-cultivated alginate hydrogel covered by a thin layer of rat muscle tissue. The sample was put in a square-shaped tube mounted with plastic foam ready for imaging.

4.2.3 Synchrotron X-ray Radiography

SR X-ray imaging was carried out on the Biomedical Imaging and Therapy (BMIT) bending magnet (BM) beamline 05B1-1, at the Canadian Light Source (CLS). BMIT can provide synchrotron-specific imaging and therapy capabilities. 05B1-1 allows either monochromatic or filtered white beam to be used in the experimental hutch. The monochromatic spectral range spans 8-40 keV. The experimental hutch also has a positioning system that allows computed tomography and planar imaging [70].

In this experiment, projection imaging methods such as absorption imaging, in-line phase contrast imaging, and diffraction-enhanced imaging (DEI) were performed at low energy level (20 keV) and high energy level (26 keV) of monochromatic beam. Three sample-to-detector distances (SD), 26.5 cm, 66.5 cm and 72 cm, were chosen to compare the effects of phase contrast and absorption contrast. A Hamamatsu C9300 (Japan) detector was chosen for use. Pixel size was 4 microns and field of view (FOV) was 7 mm.

4.2.4 Synchrotron Radiation Micro-computed Tomography

SR μCT was carried out to provide 3D visualization of brain tissue embedded inside alginate hydrogels both with and without OsO_4 staining. Sample-to-detector distances (SD) of 26.5 cm and 72 cm were set. Samples were mounted on a rotational sample stage and rotated at a step angle of 0.2^{o} over 180^{o}. Raw images were reconstructed using traditional filtered-back projection (FBP) algorithm and volume rendered in CTVox (Skyscan).

4.3 Results

4.3.1 Sample to Detector Distance (SD) Influence

Rat brain tissue embedded in alginate hydrogels and stained with 0.1% OsO_4 was imaged on BMIT beamline. To compare differences between absorption

and in-line phase contrast imaging, the sample-to-detector distances (SD) were set at 26.5 cm, 66.5 cm and 72 cm, respectively. Photon energy was set at 26 keV. Figure 22 (a)-(c) shows the results at SD1=26.5 cm, SD2=66.5 cm and SD3=72 cm respectively. When SD is small (indicating the detector is close to the sample), absorption contrast is dominant. As the distance increases, the phase contrast becomes more obvious. In Figure 22, the stripes, which indicate pieces of brain tissue, become much clearer at a longer SD, where phase contrast is dominant. More details can be observed in Figure 22(c). Grey value plots of part of the images (indicated by white line) in Figure 22 are given in Figure 23. Pitches near the edges of stripes are sharper in the phase contrast dominant image compared to the absorption image, indicating better contrast with increased SD.

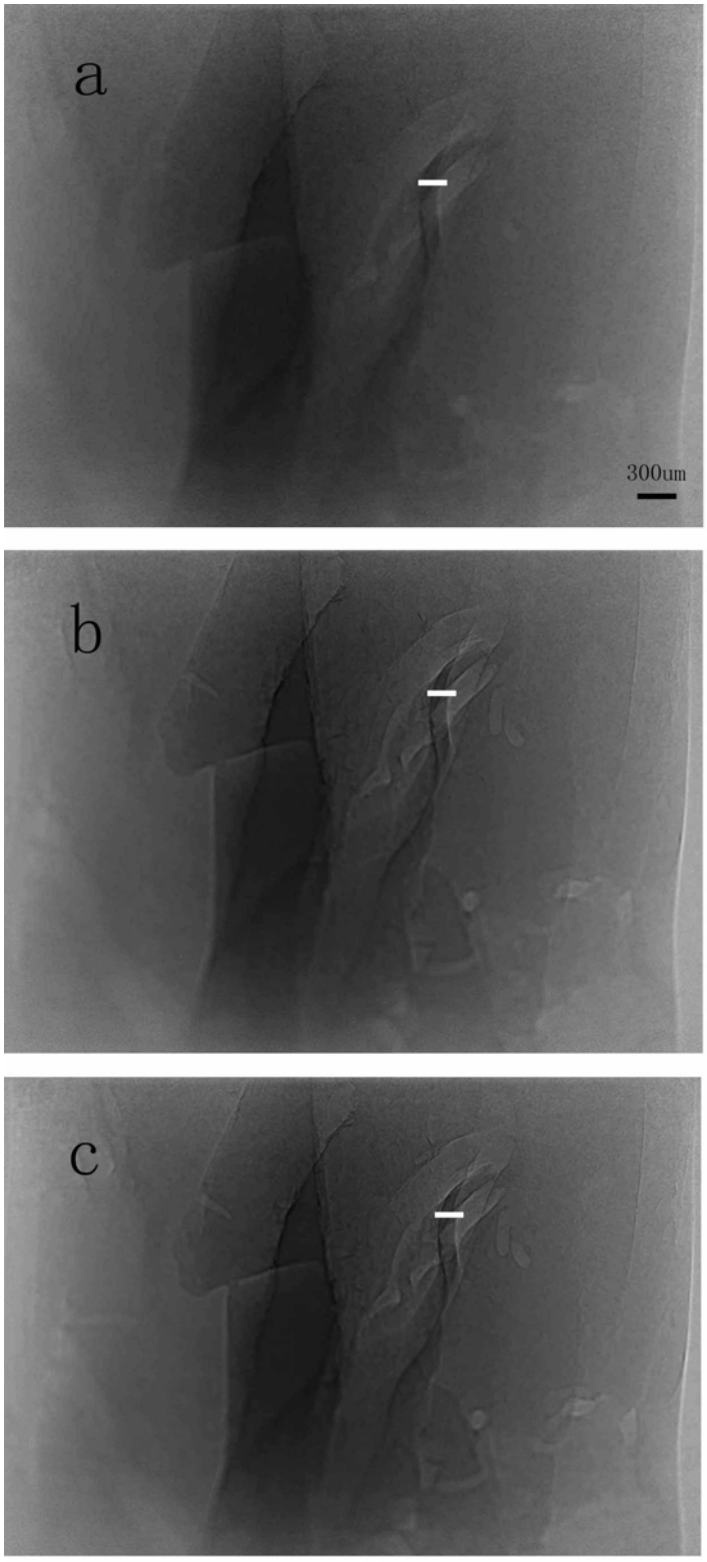

Figure 22: SR X-ray projection images with SD=26.5cm (a), 66.5 (b) and 72 (c). The stripes indicate pieces of brain tissue. Details become sharper with increased sample-to-detector distance.

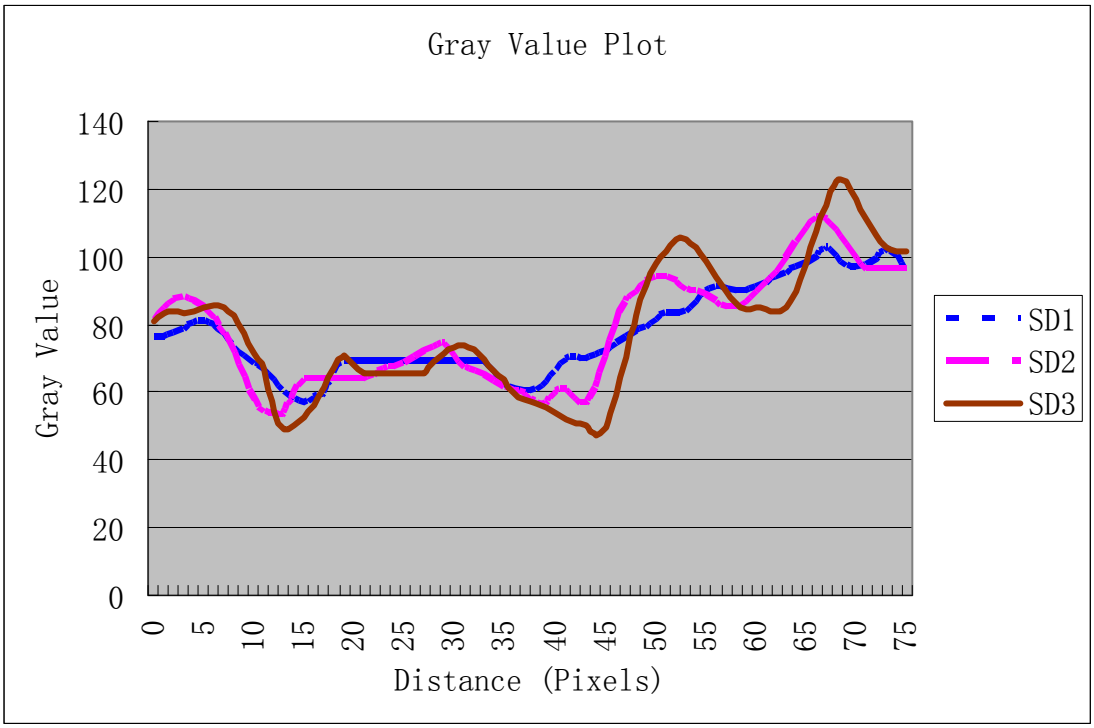

Figure 23: Gray value plots of white lines indicated in Figure 22 at three different sample-to-detector distances (SD). With a longer SD, pitches along the edges become more obvious.

4.3.2 Photon Energy Influence

In order to observe the influence of different photon energies on the quality of imaging, two photon energies, i.e., 20 keV and 26 keV, were used for imaging alginate gels buried with rat brain tissue. Samples were stained with 0.1% OsO_4. SD was set at 72 cm. Figure 24 shows the results at 26 keV (a) and 20 keV (b). Details inside alginate gels, such as stripes of brain tissue, can be observed more clearly in high energy image. This suggests high energy brings better phase contrast and less absorption contrast.

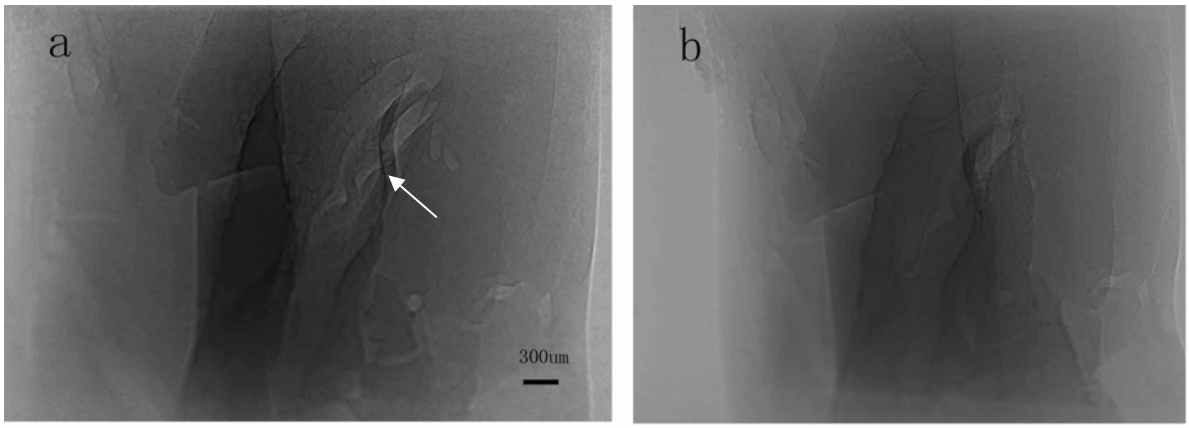

Figure 24: SR X-ray projection images at high photon energy (26keV, a) and low photon energy (20keV, b). The stripes indicate pieces of brain tissue (shown by white arrow).

4.3.3 No Osmium Staining Imaging

Phase contrast imaging enabled visualization of brain tissue embedded inside alginate gel without any osmium tetroxide staining. Figure 25 shows pieces of brain tissue inside an alginate gel which was not stained by any contrast agent as indicated by the arrow. This shows that phase contrast imaging has good visualization of soft tissue and objects with similar attenuation coefficient, which can hardly be visualized in absorption contrast imaging.

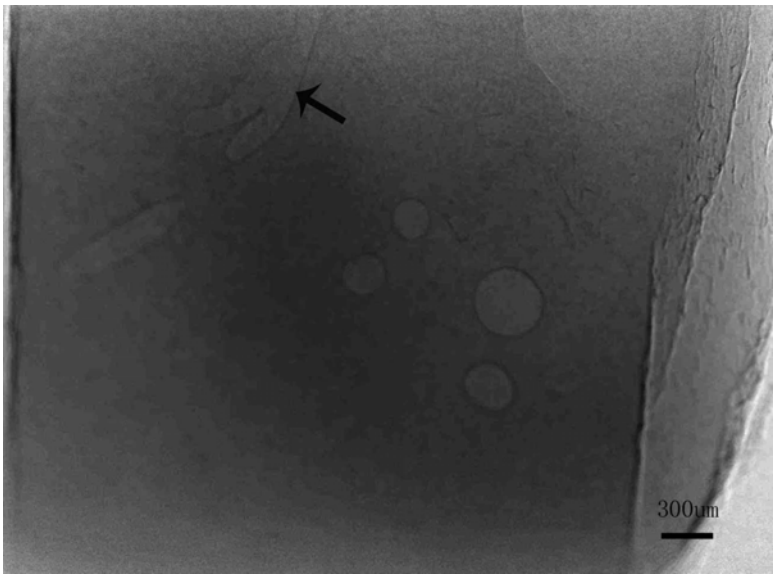

Figure 25: Phase contrast image of brain tissue buried inside alginate gels with no contrast agent. The black arrow points to a piece of brain tissue.

4.3.4 Diffraction-enhanced Imaging (DEI)

DEI is sensitive to thickness gradient of samples and has excellent performance in revealing the edges. It is an analyzer based phase contrast imaging method. For the DEI images presented in the following, photon energy was set at 20 keV.

4.3.4.1 Brain Tissue Embedded Inside Alginate Hydrogel

Brain tissue embedded inside alginate hydrogel with 0.1% OsO_4 staining was imaged using DEI technique. Three separate images were obtained at the top, low angle side and high angle side of the rocking curve. Figures 26 (a)-(c) are images from the top (a), low angle (b) and high angle (c) of rocking curve respectively. Figure 26(a) is also known as the extinction image. Extinction is the loss of intensity due to diffraction occurring as the beam traverses the object. The type of extinction referred to is commonly called secondary extinction. According to equations 1 and 2 discussed in the Background section, two resulting images, apparent absorption image (also known as intensity image) and refraction angle image, can be obtained (Figure 27). From DEI results, small strands of brain tissue can be seen, but not as many revealed as in in-line phase contrast imaging. That is mainly because thin brain tissue (200 microns) and hydrogels do not have enough thickness gradients in z-axis which prevents DEI from illustrating its strength. The sample of brain tissue inside alginate gel without osmium staining was also imaged in DEI as a comparison (Figure 28). No brain tissue can be observed, except for gel structures.

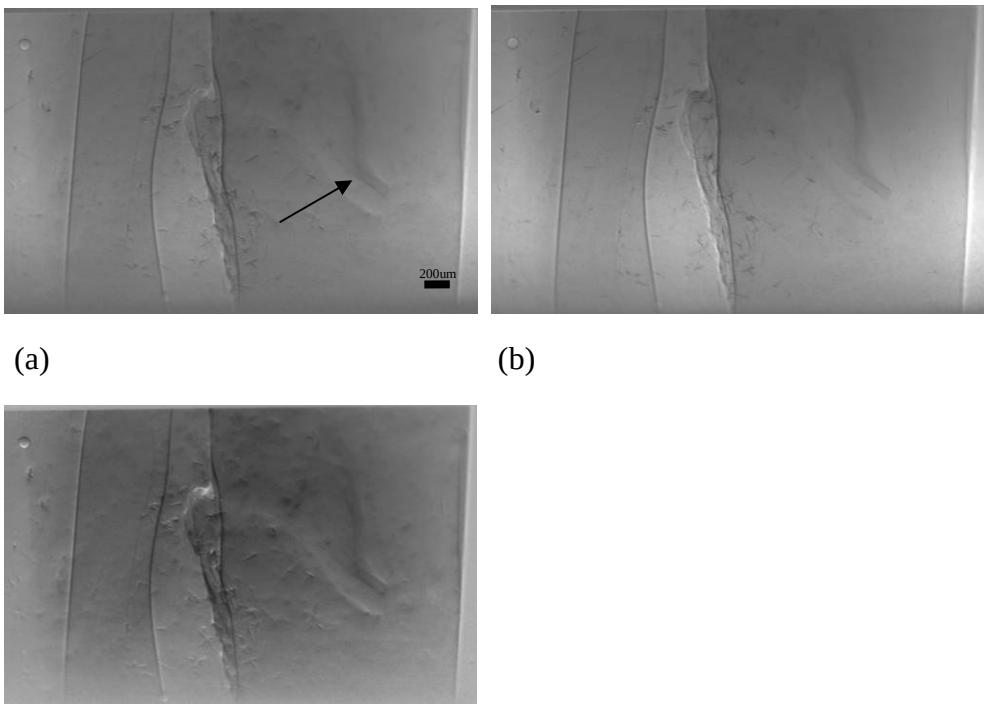

Figure 26: DEI images at top (a), low angle (b) and high angle (c) of rocking curve.

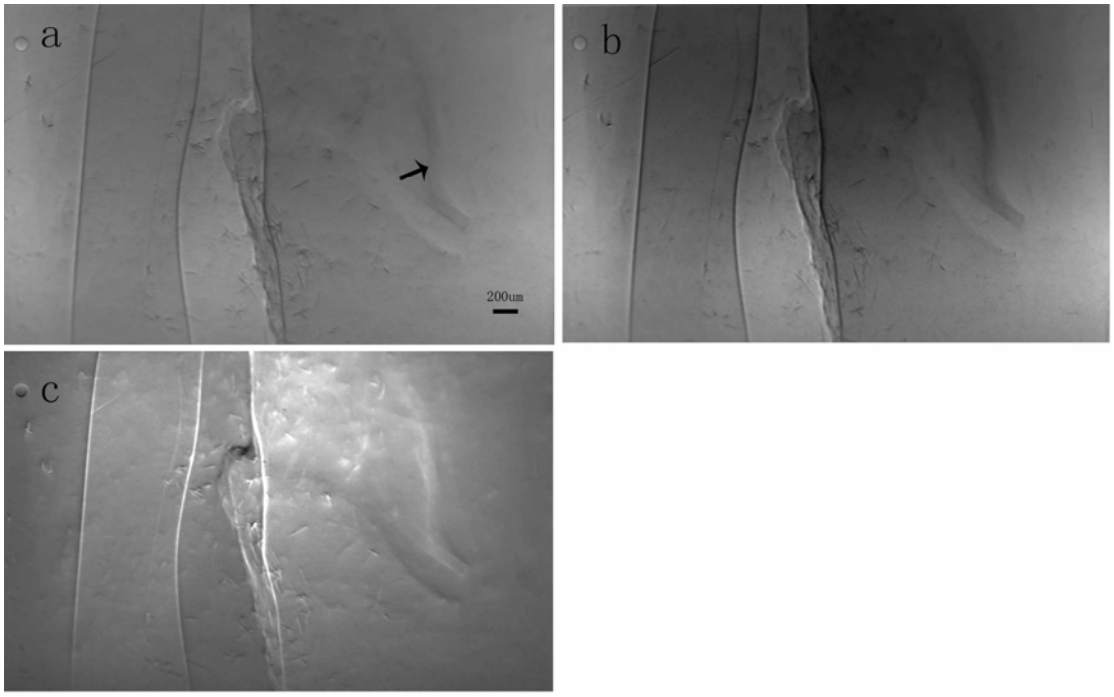

Figure 27: Extinction image (a), Intensity image (b) and Refraction Angle image (c) of rat brain tissue embedded inside alginate gels and stained with 0.1% OsO_4. Strand of brain tissue of about 100 microns in diameter is indicated by arrow. Photon energy was 20 keV.

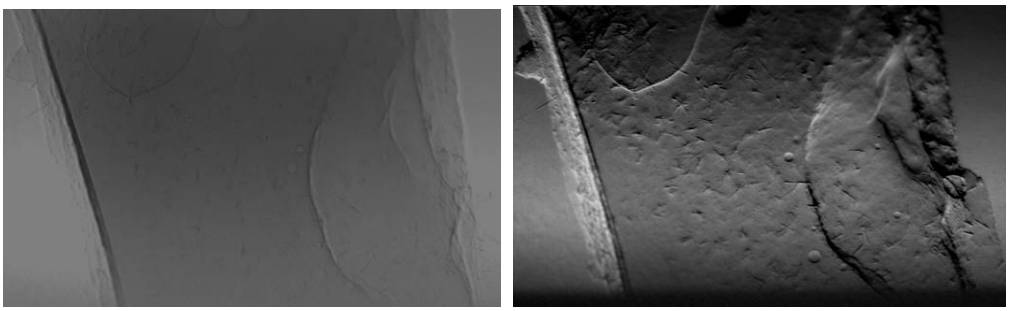

(a) (b)

Figure 28: Intensity Image (a) and Refraction Angle Image (b) of brain tissue inside alginate gel without Osmium staining.

4.3.4.2 Cell-cultivated Alginate Gel Buried in Rat Muscle Tissue

Cell-cultivated alginate gel which was cultured for 4 days was firstly stained with 0.5% osmium tetroxide and then buried inside a thin piece of rat muscle tissue. The photon energy of DEI imaging was 20 keV. From DEI results (Figure 29 a -c), the shape of the cell-cultivated gel can be clearly seen, but no cells can be visualized at this stage. Compared to DEI results, in-line phase contrast image of the same sample (Figure 29d) can barely give the outline of the buried gel. This suggests DEI has superior performance in imaging the samples with a thickness gradient.

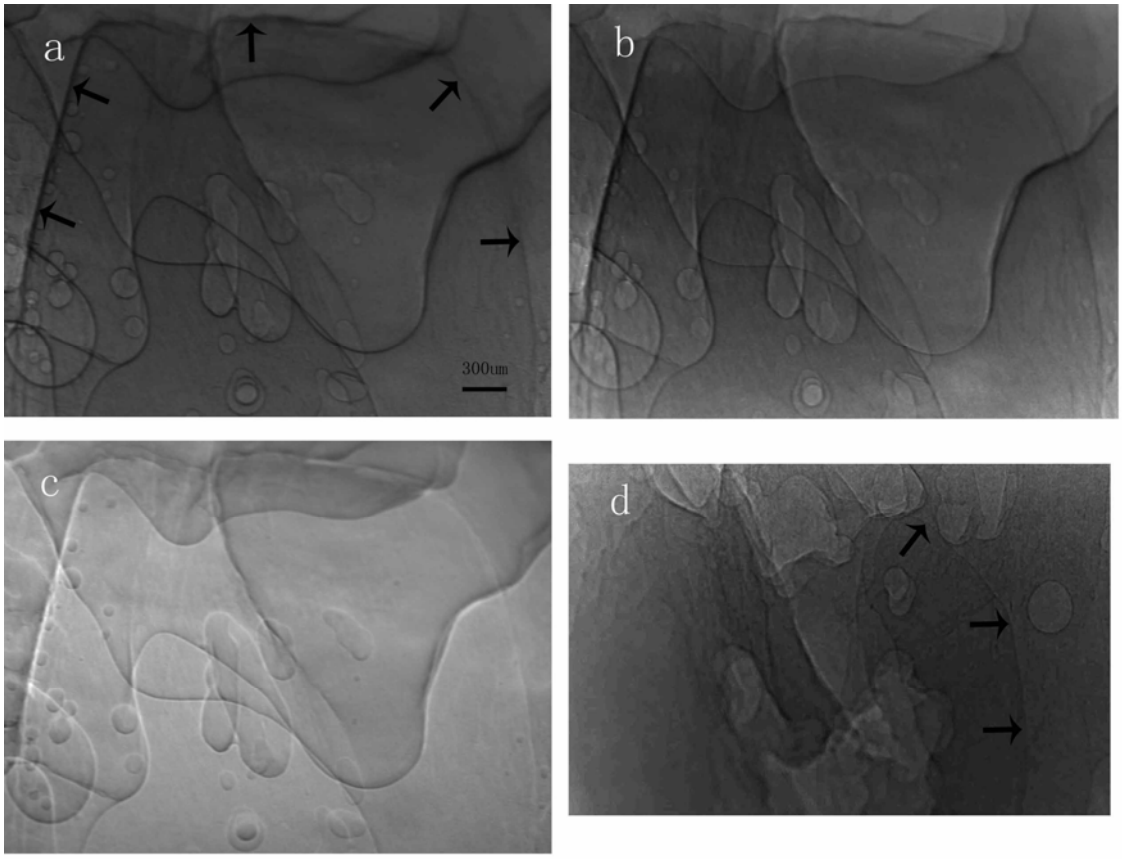

Figure 29: Extinction image (a), Intensity image (b) and Refraction Angle image (c) of cell-cultivated alginate gel (Schwann cell line, 0.5% OsO_4 staining) buried in rat muscle tissue. Photon energy was 20 keV. The edge of gel is clearly observed and indicated with arrows. Figure 29(d) is the in-line phase contrast result of the same sample. The gel edge is barely seen.

4.3.5 SR μ CT Results

SR μ CT of brain tissue embedded in alginate hydrogels both with OsO_4 staining and without OsO_4 staining were performed as a comparison using the BMIT beamline. Projections were taken at a step angle of 0.2 degrees over a total rotation angle of 180 degrees. Photon energy was set at 20 keV; and the SD was 72 cm for sample with OsO_4 staining and 26.5 cm for sample without any staining.

Figure 30 shows a slice of reconstructed image of sample with OsO_4 staining. A

Region of Interest (ROI) was taken to include the long strands of brain tissue surrounded by alginate hydrogel. In this image, brain tissue strands can be visualized, but with great difficulty. Image processing methods were applied to enhance visualization of the target, such as a medium filter to smooth the image, despeckling to remove noise, and thresholding to binarize the image and resolve desired brain tissue strands. With targeted brain tissue strands isolated out, the complete set of slices were volume rendered in CTVox (SkyScan) as shown in Figure 31. A movie with rotation of the volume was also obtained from CTVox. From the 3D result, some spots around the sample can be noticed, which are noise due to the low contrast of original image.

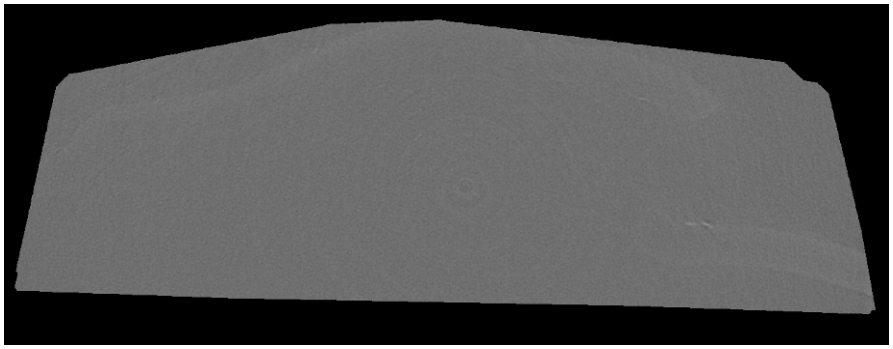

Figure 30: One slice of reconstructed images of brain tissue embedded in alginate hydrogel and with OsO_4 staining. The ROI shown here indicates the strands of brain tissue.

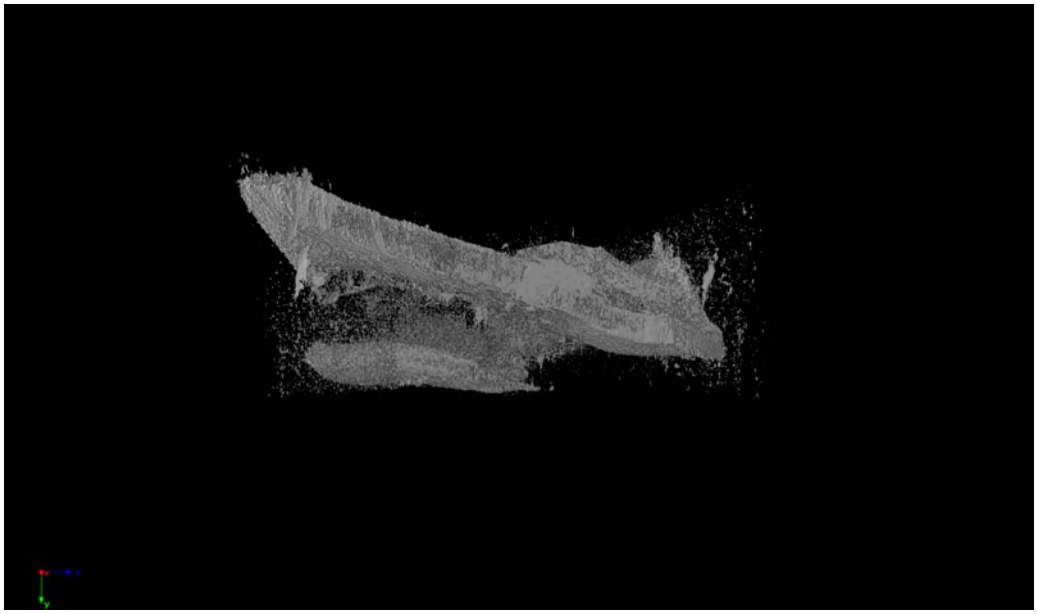

Figure 31: 3D volume rendered result of brain tissue with OsO_4 staining.

As to the sample without any OsO_4 staining, Figure 32 shows one slice of the reconstructed image. In this image, the middle rectangular structure is the alginate hydrogel put inside a round tube, filled by air. Inside the alginate hydrogel, spaces where the brain tissue is embedded can be visualized clearly. With image processing methods, the purpose is to subtract those holes and spaces for 3D rendering. Thresholding was performed to binarize the images and also despeckling to remove the noise. Then 3D volume rendering was carried out in CTVox, and the resulting image is shown in Figure 33. The large pieces and other smaller strands are all brain tissue.

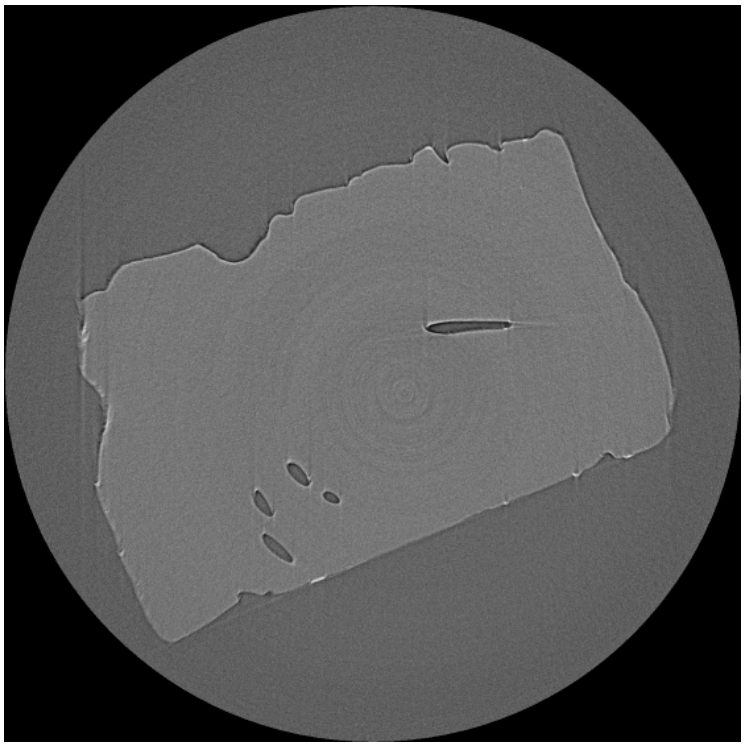

Figure 32: One slice of reconstructed images of brain tissue embedded in alginate hydrogel and with no OsO_4 staining.

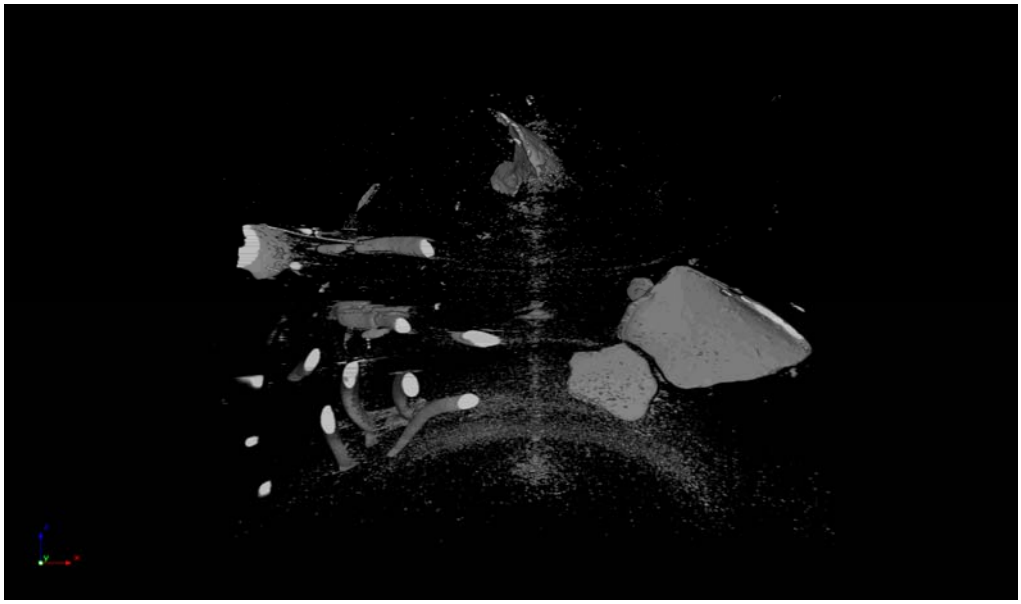

Figure 33: 3D volume rendered result of brain tissue with no OsO_4 staining.

4.4 Conclusions and Discussions

In this chapter, SR X-ray Imaging was applied in alginate hydrogels containing embedded rat brain tissue, or in hydrogels buried in rat muscle tissue. Different

imaging methods were compared. As soft tissue and alginate hydrogels have similar attenuation coefficients, absorption contrast may be too weak to distinguish among different sample features. When increasing the distance between the sample stage and the detector (sample-to-detector distance, SD), phase contrast becomes more obvious. In-line phase contrast imaging is shown to have better visualization of features with similar attenuation coefficients, even without any heavy metal staining. It produces sharper edges and greater differences in grey values. Higher photon energy is shown to have better phase contrast results. Diffraction-enhanced imaging (DEI) has strength in showing the thickness gradient inside a sample. Synchrotron radiation micro-computed tomography (SR μCT) is a novel method utilizing SR X-rays and provides 3D information about the samples.

Using the methods described in this study, no cells can be visualized using SR X-ray imaging methods. This is mainly due to the limit of actual spatial resolution of the detector, which is about four microns. However, the average size of Schwann cells grown inside alginate hydrogels is around 2 to 3 microns, smaller than the limit of pixel size. From the results of cell-material interaction experiment, Schwann cells seeded in the surrounding area of alginate hydrogels can hardly grow inside. So it is not possible to visualize clustered of Schwann cells seeded on the outside and then grow inside of alginate hydrogles. Other materials that will not swell in liquid can be tried in future work. Also from the results of experiment above, Schwann cells can stretch and cluster in a group of size larger than 30 microns. The size is possible to be visualized in SR X-ray imaging. However, the 100-micron slice of alginate hydrogel limits the merits of non-destructive X-ray imaging, which can penetrate through thick samples and even the human body. Therefore, the ultimate purpose of SR X-ray Imaging in cell-level in the future is to visualize live cells with harmless staining or even without any staining.

5. CONCLUSION, DISCUSSION AND FUTURE WORK

5.1 Conclusions

Three pieces of research work were carried out in this study. From these separate but still inter-connected experiments, several conclusions can be made regarding the structural and biological properties of alginate scaffold for use in tissue engineering.

Firstly, alginate is suitable for Schwann cells to proliferate with cells blended inside. Cells tended to grow and proliferate in alginate hydrogels as the time in culture increased. Also, they appeared to have more chance of exchanging of nutrients and wastes in thin slice of alginate hydrogels, thus growing more rapidly and stretching in rod shape. The shape and clustering of Schwann cells in thin slices of alginate gel were much like the growth observed in pure medium. Although some research groups have reported alginate as a suitable matrix for Schwann cells [71, 72], study of cells embedded in thin slices of alginate gels should be the novelty of this research work. As a hydrogel, alginate scaffold has pores too small for cells to move inside. However, as a freeze-dried scaffold, alginate scaffold has structural parameters very suitable for cells to be seeded. The pore size, porosity and interconnectivity are shown to be good for tissue engineered scaffold.

Secondly, the novel micro-CT imaging technique can be used in the characterization of alginate scaffolds with low absorption contrast and similar density to that of soft tissue. As a non-destructive and non-invasive method, micro-CT requires simple or even no sample preparation process compared to other traditional methods such as SEM or light microscopy. For traditional methods, samples are usually sectioned to thin slices in order to see the inside. That may cause damage to the target structure inside samples. Micro-CT utilizes different absorption attenuation coefficients of samples to visualize the details

inside. It can also provide 3D rendered models and 3D analysis. From the research work in this thesis, micro-CT shows great merits in characterization of material properties of freeze-dried alginate scaffolds with different alginate concentrations and freezing temperatures.

Thirdly, the application of SR X-ray imaging techniques in visualization of alginate hydrogels with soft tissue shows the promising future of medical imaging of low absorption contrast biological sample using DEI and in-line phase contrast imaging even without any staining material. Soft tissue usually has similar density and absorption attenuation coefficient of alginate hydrogels, and it can be difficult to visualize using traditional X-rays coming from an X-ray tube. Taking advantage of the high flux and monochromatic Synchrotron X-rays, in-line phase contrast imaging was performed in the present work, and compared with the results of absorption contrast imaging. With increased sample-to-detector distance, in-line phase contrast was more obvious, thus revealing more details of soft tissue imbedded inside alginate gels than absorption imaging. Also, higher photon energy enabled more visualization of sample details in in-line phase contrast imaging. In-line phase contrast imaging could also visualize strands of brain tissue inside the alginate gel without osmium staining. Diffraction-enhanced imaging (DEI) is an analyzer-based phase contrast imaging technique and is shown to be excellent in determining the thickness gradient of soft tissue samples. Although the process of DEI is a little bit more complex, as it requires processing of two images obtained at both the low and high angle side of the rocking curve, the resolution of edges is much better than other methods. SR μCT is the combination of SR X-ray imaging with computed tomography to provide 3D information inside samples without any sectioning. Movies can be made to show the samples rotating through different orientations and give full visualization of the features.

5.2 Limitations of The Present Work

The thesis work was subject to the following limitations:

a) This work does not include a traditional evaluation method of porosity more accurate than SEM, for instance, the nitrogen porosimeter, as a comparison to micro-CT results. As freeze-dried alginate scaffolds are too light (around 100 mg) for the weight limit of nitrogen porosimeter (200 mg), nitrogen porosimeter cannot be applied here.

b) Cell culture experiment was carried out with 4% sodium alginate concentration crosslinked with 2% calcium chloride ($CaCl_2$). Cell proliferation under other concentrations of alginate and $CaCl_2$ was not included. This work mainly focused on X-ray imaging of alginate hydrogels, so solid gels were of great concerns. 4% sodium alginate when crosslinked with 2% $CaCl_2$ could produce a good shape of solid gels for imaging.

c) As cell size was beyond the spatial resolution (around 4 microns) of synchrotron radiation (SR) X-ray imaging, and also as cells did not cluster during proliferation, till this stage, imaging of individual cells was not possible, even with heavy metal staining such as osmium tetroxide (OsO_4).

5.3 Future Work

Due to the limitations of the present work, much can be carried out in the future. For instance, in characterization of the structural properties of freeze-dried alginate scaffolds, SEM was used to provide supporting descriptive and analytical information in 2D, but more quantitative information in 3D is required to support the 3D analysis results of micro-CT. Some of the traditional evaluation methods, such as Mercury porosimeter, can be carried out.

In this work, cell-material interaction was carried out only with 4% sodium alginate solution crosslinked with 2% $CaCl_2$. Other combination of sodium alginate concentration and $CaCl_2$ concentration can be tried in the future for the study of cell proliferations. Higher concentration of sodium alginate solution will

be better for cell growth, but with much more difficulties to dissolve alginate powder. Usually alginate solution of higher than 7% needs to be heated to dissolve. On the other hand, lower concentration of $CaCl_2$ will introduce less Ca^{2+} ions that may disturb the ionic balance across the cell membrane. Different combinations can be tried in the future to find a most suitable one to crosslink and cultivate cells.

In SR X-ray imaging, the sample-to-detector distance (SD) was set furthest at 72 cm. Due to the set up of the beamline, no greater distance can be reached at this stage. Usually for in-line phase contrast imaging, SD greater than 1 m will have better phase contrast and eliminate absorption contrast. Therefore, in the future, SD larger than 1 m can be tried on BMIT beamline.

The imaging of cells can still not be achieved with the novel SR X-ray imaging technique. This is mainly because in thick alginate hydrogels, cells did not cluster. The individual cell size is just about the pixel size of 4 microns, and is therefore beyond the spatial resolution. In the future, BMIT beamline will have detectors with higher resolution, down to 2 microns. But that may still not be able to image individual cell of 2 to 3 microns. So cells seeded rather than blended inside can be tried with other biomaterials not as swollen in water as alginate hydrogel. Poly(e-caprolactone) (PCL) can be used as it is not swollen in water and have pores large enough for cells to penetrate through. When cells are seeded on top of the PCL scaffold, they can proliferate in clusters and grow through pores into the scaffold. The clustered cells with larger aggregate size can possibly be visualized in SR X-ray Imaging. OsO_4 can be used to stain the cell membrane.

References:

1. Langer R and Vacanti J.P. , *Tissue Engineering.* Science 260(5110):920-926, 1993.
2. Rattner DW et. al., *Beyond the laparoscope: Minimally invasive surgery in the new millennium.* . Surgeray 125(1): 19-22, 1999.
3. Vacanti JP& Langer R. , *Tissue Engineering: the design and fabrication of living replacement devices for surgical reconstruction and transplantation.* Lancet 354(SI32-SE34),1999.
4. *Tissue Engineering.* Academic Press, 2008.
5. Rowley JA et. al., *Alginate hydrogels as synthetic extracellular matrix materials.* Biomaterials 1999; 20(1):45-53.
6. Kataoka K et. al., *Alginate enhances elongation of early regenerating axons in spinal cord of young rats.* Tissue Engineering 2004;10(3-4):493-504.
7. Gianluca Turco et. al., *Alginate/Hydroxyapatite Biocomposite For Bone Ingrowth: A trabecular Structure With High And Isotropic Connectivity.* Biomacromolecules 2009, 10, 1575-1583.
8. Prang P et. al., *The promotion of oriented axonal regrowth in the injured spinal cord by alginate-based anisotropic capillary hydrogels.* Biomaterials 2006; 27(19):3560-9.
9. Saif Khalil, W.S., *Bioprinting Endothelial Cells With Alginate for 3D Tissue Constructs,*. J. of Biomechanical Engineering, Nov. 2009, Vol.131, 111002-3.
10. M.G. Li et. al., *A brief review of dispensing-based rapid prototyping techniques in tissue scaffold fabrication: role of modeling on scaffold properties prediction.* Biofabrication 1 (2009) 032001 (10pp).
11. Sachlos, E. et. al., *Making tissue engineering scaffolds work. Review on the application of solid freeform fabrication technology to the production of tissue engineering scaffolds.* Eur. Cells Mater. 2003. 5, 29-40.
12. Hutmacher, D.W., *Scaffolds in Tissue Engineering Bone and Cartilage.* Biomaterials 21: 2529-2543, 2000.
13. H. Tabesh, et. al., *The role of biodegradable engineered scaffolds seeded with Schwann cells for spinal cord regeneration.* Neurochemistry International 54 (2009) 73-83.
14. Simon P. Frostick, et. al., *Schwann cells, neurotrophic factors, and peripheral nerve regeneration.* Microsurgery 18:397-405, 1998.
15. Oatley, C.W., Sir, *The Scanning Electron Microscope.* Cambridge University Press, London, 1972.
16. Hsieh, J., *Computed Tomography: Principles, Design, Artifacts, and Recent Advances.* SPIE, 2003.
17. Simon Young, et. al., *Microcomputed Tomography Characterization of Neovascularization in Bone Tissue Engineering Applications.* Tissue Engineering 2008;14, 295-306.
18. B.D. Arhatari et al, *Phase contrast radiography: Image modeling and*

optimization. Review of Scientific Instruments, Vol.75, No. 12, Decemeber 2004.

19. Michio Kono et al, *Refraction Imaging and Histologic Correlation in Excised Tissue from a Normal Human Lung: Preliminary Report.* Acad Radiol Vol 8, No 9, Septermber 2001.
20. P. Liu et. al, *Morphological Study of Early Stages of Lung Cancer Using Synchrotron Radiation.* J Synchrotron Radiat. 2008 Jan ;15 (Pt 1):36-42 18097076.
21. P. Liu et. al, *Detection of Lung Cancer with Phase-Contrast X-ray Imaging Using Synchrotron Radiation.* pp.2001-2004,28th IEEE Proceedings EMBS, 2006.
22. D. Chapman et. al, *Diffraction Enhanced X-ray Imaging.* Phys. Med. Biol. 42(1997) 2015-2025.
23. Gao X et. al, *A micro-tomography method based on X-ray diffraction enhanced imaging for the visualization of micro-organs and soft tissues.* Comput Med Imaging Graphics (2006).
24. ED Pisano et. al, *Human breast cancer specimens diffraction-enhanced imaging with histologic correlation-improved conspicuity of lesion detail compared with digital radiography.* Radiology, 2000, 214(3):895.
25. R A Lewis et. al, *X-ray refraction effects: application to the imaging of biological tissues.* The British Journal of Radiology, 76 (2003), 301-308.
26. R.H. Menk et. al, *Diffraction-enhanced X-ray medical imaging at the ELETTRA synchrotron light source.* Nuclear Instruments and Methods in Physics Research A 548(2005)213-220.
27. Phllips, J.B. et. al., *Neural tissue engineering: a self-organizing collagen guidance conduit.* Tissue Engineering 2005;11, 1611-1617.
28. Matin, S., *Spinal cord regeneration via collagen entubulation.* Thesis. Department of Aeronautics and Astronautics, John Hopkins University, Massachuset Institute of Technology, 2004.
29. Ying Yuan et. al., *The interaction of Schwann cells with chitosan membranes and fibers in vitro.* Biomaterials 25 (2004) 4273-4278.
30. Haipeng, G., *Studies on nerve cell affinity of chitosan-derived materials.* Journal of Biomedical Materials Research 52 (2), pp.285-295.
31. Kim, K. et. al.,*Control of degradation rate and hydrophilicity in electrospun non-woven poly($_{D,L}$-lactide) nanofiber scaffolds for biomedical applications.* Biomaterials 24 (2003) 4977-4985.
32. Hurtado, A. et. al., *Poly($_{D,L}$-lactic acid) macroporous guidance scaffolds seeded with Schwann cells genetically modified to secrete a bi-functional neurotrophin implanted in the completely transected adult rat thoracic spinal cord.* Biomaterials 2006; 27, 430-442.
33. Schnell, E. et. al., *Guidance of glial cell migration and axonal growth on electrospun nanofibers of poly-e-caprolactone and a collagen/poly-e-caprolactone blend.* Biomaterials 2007; 28, 3012-3025.
34. Venugopal, J. et. al., *In vitro study of smooth muscle cells on polycaprolactone*

and collagen nanofibrous matrices. Cell Biol. Int. 25, 861-867.

35. Chang, S.C. et. al., *Injection moding of chondrocyte/alginate constructs in the shape of facial implants.* Journal of Biomedical Materials Research 2001 55 (4), pp.503-511.
36. Guo, J. et. al.,*Culture and growth characteristics of chondrocytes encapsulated in alginate beads.* Connective Tissue Research, 1989, 19:277-297.
37. P. Malafaya et. al., *Morphology, mechanical characterization and in vivo neo-vascularization of chitosan particle aggregated scaffolds architectures,.* Biomaterials 29 (2008) 3914-3926, 2008.
38. Lin ASP et. al., *Microarchitecture and mechanical characterization of oriented porous polymer scaffolds,.* Biomaterials 24 (2003) 481-9.
39. Laurence M. Mathieu, et. al.,*Architecture and properties of anisotropic polymer composite scaffolds for bone tissue engineering,.* Biomaterials 27 (2006) 905-916.
40. Wang F. et. al., *Precision extruding deposition and characterization of cellular poly-caprolactone tissue scaffolds,.* Rapid Prototyping J 2004; 10(1):42-9.
41. Reto Meuli et. al, *Synchrotron radiation in radiology: radiology techniques based on synchrotron sources.* Eur Radiol (2004) 14:1550-1560.
42. A. Peterzol et. al, *Performance of the K-Edge Digital Subtraction Angiography imaging system at the European Synchrotron Radiation Facility Radiation Protection Dosimetry.* doi:10.1093/rpd/nci710 (2006).
43. Yamashita T et. al, *Evaluation of the Microangioarchitecture of Tumors by Use of Monochromatic X-Rays,.* Investigative Radiology, 2001 Volume 36, Number 12, 713-720.
44. Toshihiro SERA et. al., *3D visualization of intact mouse lung by synchrotron radiation CT,.* Proceedings of the 26th Annual International Conference of the IEEE EMBS 2004.
45. Momose A & Fukuda J., *Phase-contrast radiographs of nonstained rat cerebellar specimen.* Med Phys 1995; 22: 375-379.
46. Takeda T et. al, *Phase-contrast imaging with synchrotron X-rays for cancer lesion.* Acad Radiol 1995; 2: 799-803.
47. E. Castelli et. al, *Clinical mammography at the SYRMEP beam line.* Nuclear Instruments and Methods in Physics Research A 572 (2007) 237-240.
48. Fulvia Arfellia et. al., *Synchrotron Radiation Mammography: Clinical Experimentation.* CP879, Synchrotron Radiation Instrumentation: Ninth International Conference.
49. T. Takeda et. al, *Iodine imaging in thyroid by fluorescent X-ray CT with 0.05mm spatial resolution.* Nuclear Instruments and Methods in Physics Research A 467-468 (2001) 1318-1321.
50. Tohoru Takeda et. al., *Phase-contrast and fluorescent X-ray imaging for biomedical researches.* Nuclear Instruments and Methods in Physics Research A 548(2005)38-46.
51. Jin Wu et. al, *Fusion imaging of fluorescent and phase-contrast X-ray*

computed tomography using synchrotron radiation in medical biology,. Proc. Of SPIE Vol.6318,631828(2006).

52. F. Peyrin et.al., *SEM and 3D Synchrotron Radiation Micro-Tomography in the Study of Bioceramic Scaffolds for Tissue-Engineering Applications.* Biotechnology and Bioengineering, Vol.97,No.3, June 15,2007.
53. P. Thurner et.al., *Tomography studies of biological cells on polymer scaffolds.* J.Phys.:Condens. Matter 16 (2004) S3499-S3510.
54. M. Mastrogiacomo et.al., *Synchrotron Radiation Microtomography of Bone Engineered from Bone Marrow Stromal Cells.* Tissue Engineering, Volume 10, Number 11/12, 2004.
55. Philipp Thurner et. al, *Tomography studies of human foreskin fibroblasts on polymer yarns.* Nuclear Instruments and Methods in Physics Research B 200 (2003) 397-405.
56. P. Thurner et.al., *3D Morphology of Cell Cultures: A Quantitative Approach Using Micrometer Synchrotron Light Tomography.* Microscopy Research and Technique 66:289-298 (2005).
57. Hermann Seitz et.al, *Three-Dimensional Printing of Porous Ceramic Scaffolds for Bone Tissue Engineering.* J. Biomed Mater Res Part B: Appl Biomater 74B: 782-788, 2005.
58. Zein I et. al., *Fushed deposition modeling of novel scaffold architectures for tissue engineering applications.* Biomaterials 2002; 23:1169-85.
59. Sylvain Deville et. al., *Freeze casting of hydroxyapatite scaffolds for bone tissue engineering.* Biomaterials 27 (2006) 5480-5489.
60. Biman B. Mandal et. al., *Cell proliferation and migration in silk fibroin 3D scaffolds.* Biomaterials 30 (2009) 2956-2965.
61. Saey T. Ho, D.W.H., *A Comparison of micro CT with other techniques used in the characterization of scaffolds,*. Biomaterials 27 (2006) 1362-1376, 2006.
62. Cohen D.L., et. al., *Improved quality of 3D-printed tissue constructs through enhanced mixing of alginate hydrogels.* Proceedings of the 19th Annual Solid Freeform Fabrication Symposium, Austin TX, Aug 2008.
63. K.F. Leong et. al., *Solid Freeform Fabrication of Three-Dimensional Scaffolds for Engineering Replacement Tissues and Organs.* Biomaterials 2003; 24(13):2363-2378.
64. T.M. Freyman et. al., *Cellular Materials as Porous Scaffolds for Tissue Engineering.* Prog. Mater. Sci., 46(3-4), pp.273-282.
65. Robinson B. et. al., *Calvarial bone repair with porous D,L-polylactide.* Otolaryng Head Neck 1995;112(6):707-13.
66. Boyan BD et. al., *Role of material surfaces in regulating bone and carilage cell response.* Biomaterials 1996; 17(2):137-46.
67. Yannas IV et. al., *Synthesis and characterization of a model extracellular matrix that induces partial regeneration of adult mammalian skin.* Proc Natl Acad Sci USA 1989;86:933.
68. Kim SS et. al., *Survival and function of hepatocytes on a novel three-dimensional synthetic biodegradable polymer scaffold with an intrinsic*

network of channels. Ann Surg 1998;228(1):8-13.

69. Shauna M. Dorsey et. al., *X-ray microcomputed tomography for the measurement of cell adhesion and proliferation in polymer scaffolds.* Biomaterials 30 (2009) 2967-2974.
70. Tomasz W. Wysokinski et. al., *Beamlines of the biomedical imaging and therapy facility at the Canadian light source -- Part 1.* Nuclear Instruments and Methods in Physics Research A 582 (2007) 73-76.
71. Suzuki, K. et. al., *Regeneration of transected spinal cord in young adult rats using freeze-dried alginate gel.* NeuroReport 10(14), pp.2891-2894, 1999.
72. Mosahebi, A. et. al., *A novel use of alginate hydrogel as Schwann cell matrix.* Tissue Engineering 7 (5), pp. 525-534, 2001.

APPENDIX A: SUPPLIEMENTARY INFORMATION

Attached to this thesis is a CD containing two videos of 3D volume rendered results. Screen-shots of the videos are shown in Figure 31 and 33 respectively.